1. Report No. FHWA/TX-83/24+306-1	2. Government Accession No.	3. Recipient's Catalog No.
4. Title and Subtitle FATIGUE BEHAVIOR OF WELDED JOINTS SUBJECTED TO VARIABLE AMPLITUDE STRESSES		5. Report Date October 1983
		6. Performing Organization Code
7. Author's) John M. Joehnk, Karl H. Frank, and Joseph A. Yura		8. Performing Organization Report No. Research Report 306-1
9. Performing Organization Name and Address Center for Transportation Research The University of Texas at Austin Austin, Texas 78712-1075		10. Work Unit No.
		11. Contract or Grant No. Research Study 3-5-81-306
12. Sponsoring Agency Name and Address Texas State Department of Highways and Public Transportation; Transportation Planning Division P. O. Box 5051 Austin, Texas 78763		13. Type of Report and Period Covered Interim
		14. Sponsoring Agency Code

15. Supplementary Notes
Study conducted in cooperation with the U. S. Department of Transportation, Federal Highway Administration. Research Study Title: "Determination of the Influence of Low Level Stress Ranges on the Fatigue Performance of Steel Weldments"

16. Abstract

The fatigue behavior of welded steel tees loaded in cantilever bending was examined using simple variable amplitude stress waveforms. These waveforms were developed by superimposing two sine wave signals, i.e., a high frequency/low amplitude signal upon a low frequency/high amplitude signal. The test program involved changing the relative size and frequency of these two sine signals. The goal of these tests was to determine the effect that smaller high frequency stress cycles would have upon the fatigue life associated with a major stress cycle.

The results of the tests indicated that the damage effect of these smaller stresses was greater than anticipated. In fact, the current AASHTO method of bridge fatigue design may be inadequate because of the damage associated with these additional stresses. The current AASHTO design practice considers only one cycle per vehicle. The smaller dynamic oscillations of the structure are ignored. The impact fraction included in design only accounts for the increase in maximum stress. The influence of the smaller cycles can be included in design by increasing the impact fraction to account for their fatigue damage. The future tests in this project using measured stress histories will be used to develop this approach.

17. Key Words welded joints, stress, variable amplitude, fatigue life, waveforms, bridges	18. Distribution Statement No restrictions. This document is available to the public through the National Technical Information Service, Springfield, Virginia 22161.
19. Security Classif. (of this report) Unclassified	20. Security Classif. (of this page) Unclassified	21. No. of Pages 97	22. Price

Form DOT F 1700.7 (8-69)

FATIGUE BEHAVIOR OF WELDED JOINTS SUBJECTED TO

VARIABLE AMPLITUDE STRESSES

by

John M. Joehnk
Karl H. Frank
and
Joseph A. Yura

Research Report Number 306-1

Determination of the Influence of Low Level Stress Ranges on
the Fatigue Performance of Steel Weldments

Research Project 3-5-81-306

Conducted for

Texas
State Department of Highways and Public Transportation

In cooperation with the
U. S. Department of Transportation
Federal Highway Administration

by the

CENTER FOR TRANSPORTATION RESEARCH
BUREAU OF ENGINEERING RESEARCH
THE UNIVERSITY OF TEXAS AT AUSTIN

October 1983

The contents of this report reflect the views of the authors, who are responsible for the facts and the accuracy of the data presented herein. The contents do not necessarily reflect the official views or policies of the Federal Highway Administration. This report does not constitute a standard, specification, or regulation.

ABSTRACT

The fatigue behavior of welded steel tees loaded in cantilever bending was examined using simple variable amplitude stress waveforms. These waveforms were developed by superimposing two sine wave signals, i.e., a high frequency/low amplitude signal upon a low frequency/high amplitude signal. The test program involved changing the relative size and frequency of these two sine signals. The goal of these tests was to determine the effect that smaller high frequency stress cycles would have upon the fatigue life associated with a major stress cycle.

The results of the tests indicated that the damage effect of these smaller stresses was greater than anticipated. In fact, the current AASHTO method of bridge fatigue design may be inadequate because of the damage associated with these additional stresses. The current AASHTO design practice considers only one cycle per vehicle. The smaller dynamic oscillations of the structure are ignored. The impact fraction included in design only accounts for the increase in maximum stress. The influence of the smaller cycles can be included in design by increasing the impact fraction to account for their fatigue damage. The future tests in this project using measured stress histories will be used to develop this approach.

IMPLEMENTATION

The results of this phase of the study cannot be directly implemented into current design practice. However, they will for a part of the basis for suggested revisions to current bridge practice in the final report.

The report is of immediate interest to engineers assessing the fatigue life of bridges or other structures from recorded stress histories. The non-linear damage model or Gurney's damage model should be employed to evaluate these stress histories. Employing the commonly used linear damage model of Miner will result in unconservative life predictions.

CONTENTS

LIST OF TABLES

LIST OF FIGURES

ix

LIST OF FIGURES (continued)

LIST OF FIGURES (continued)

NOTATION

a	Crack depth
a_f	Final crack depth
Δa	Amount of crack extension
A	Intercept of log-log S-N curve
D	Total damage as fraction of fatigue life
D_i	Fractional Damage due to n_i cycles of stress S_i
I	AASHTO impact fraction
L	Span length of bridge
L'	Distance from knife edge to weld toe on test specimen
m	Slope of constant amplitude log-log S-N curve
n	Power term of an effective stress expression
n_i	Number of cycles at S_i
N	Cycles to failure of a complex waveform
N_i	Cycles to failure of stress S_i
N_c	Cycles to failure under constant amplitude loading, σ
N_g	Predicted fatigue life using S_{rg}
N_m	Predicted fatigue life using S_{re} based on Miner's rule
N_n	Predicted fatigue life using S_{re} based on non-linear Miner's rule
N_t	Total cycles to failure
$\Delta N'$	Additional cycles needed to grow specimen crack to mid-section
N_{avg}	Predicted average fatigue life
N_{rms}, N_{rmc}	Cycles to failure of S_{rms}, S_{rmc}
p	z/σ
P_{ij}	$S_j/S_{max,i}$

S	Section modulus
S_i, S_j	Stress level i, j
S_{re}	Effective stress range
$S_{max,i}$	S_{max} or σ of a complex cycle i.
S_{rg}	Effective stress based on Gurney's cycle life interaction expression, eqn. 1.27
S_{Rminor}	Effective stress of minor cycles, z, in SS waveform
S_{Rmajor}	Effective stress of major cycles, σ, in SS waveform
z	Stress range of excursion from main constant amplitude cycle
z'	See Fig. 1.7
z_{eff}	The value of "z" which produces the same damaging effect as a constant amplitude stress z_{eff}
α_j, α_{ij}	Occurrence of S_j, S_{ij}
γ_i	n_i/N
γ_σ, γ_z	Fractional occurrence of σ, z
σ	Maximum stress range in a complex stress cycle

CHAPTER 1: INTRODUCTION

1.1 PROBLEM STATEMENT

In a recent research program at The University of Texas at Austin, stresses generated from truck loading on a bridge were monitored [5]. As the speed of the test truck increased, the maximum stress range increased. Associated with the major measured stress cycle are many smaller stress fluctuations. These smaller stress fluctuations become sizable with increased speed. This is shown in Fig. 1.1 for a truck moving across the bridge at 5 and 50 MPH.

Current AASHTO bridge fatigue specifications associate one cycle of stress for each passage of a truck over longitudinal members. The stress range produced by the design truck loading is increased by an impact fraction, I, based on the span length, L, as follows:

$$I = \frac{50}{L + 125} \tag{1.1}$$

where "I" can not exceed 30 per cent. This impact fraction is used to account for the increase in the maximum stress which occurs from the dynamic loading in a bridge as graphically shown in Fig. 1.2.

There is concern that the impact fraction, I, defined in the AASHTO specification is inadequate as the impact fraction does not directly account for the possible damage due to the additional stress cycles associated with a truck loading. The amount of damage that occurs from these additional stress cycles is not known.

Damage associated with a stress cycle, such as shown in Fig. 1.1, is normally accounted for by a linear cumulative damage rule. The

1
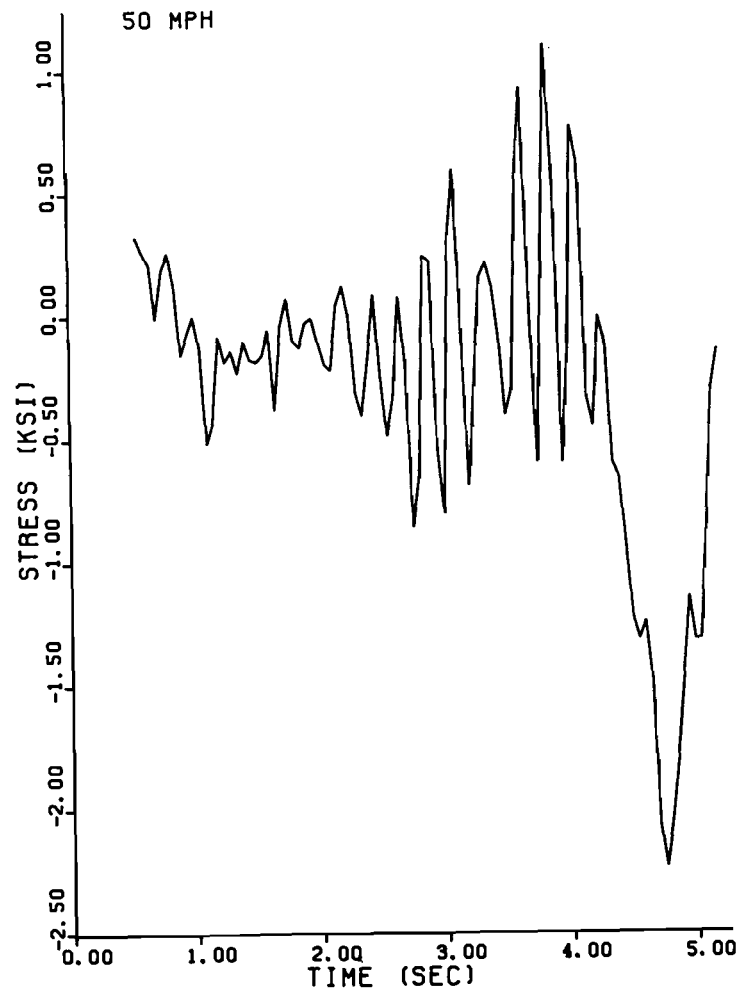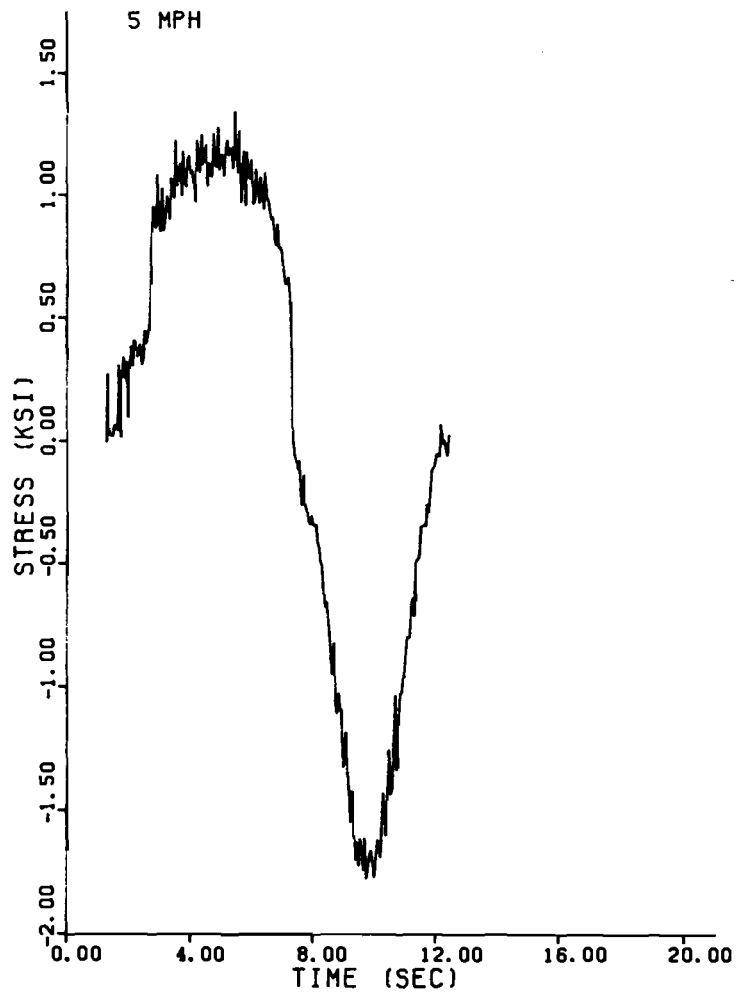
Figure 1.1   Bridge stress history for a truck velocity of 5 and 50 mph

2
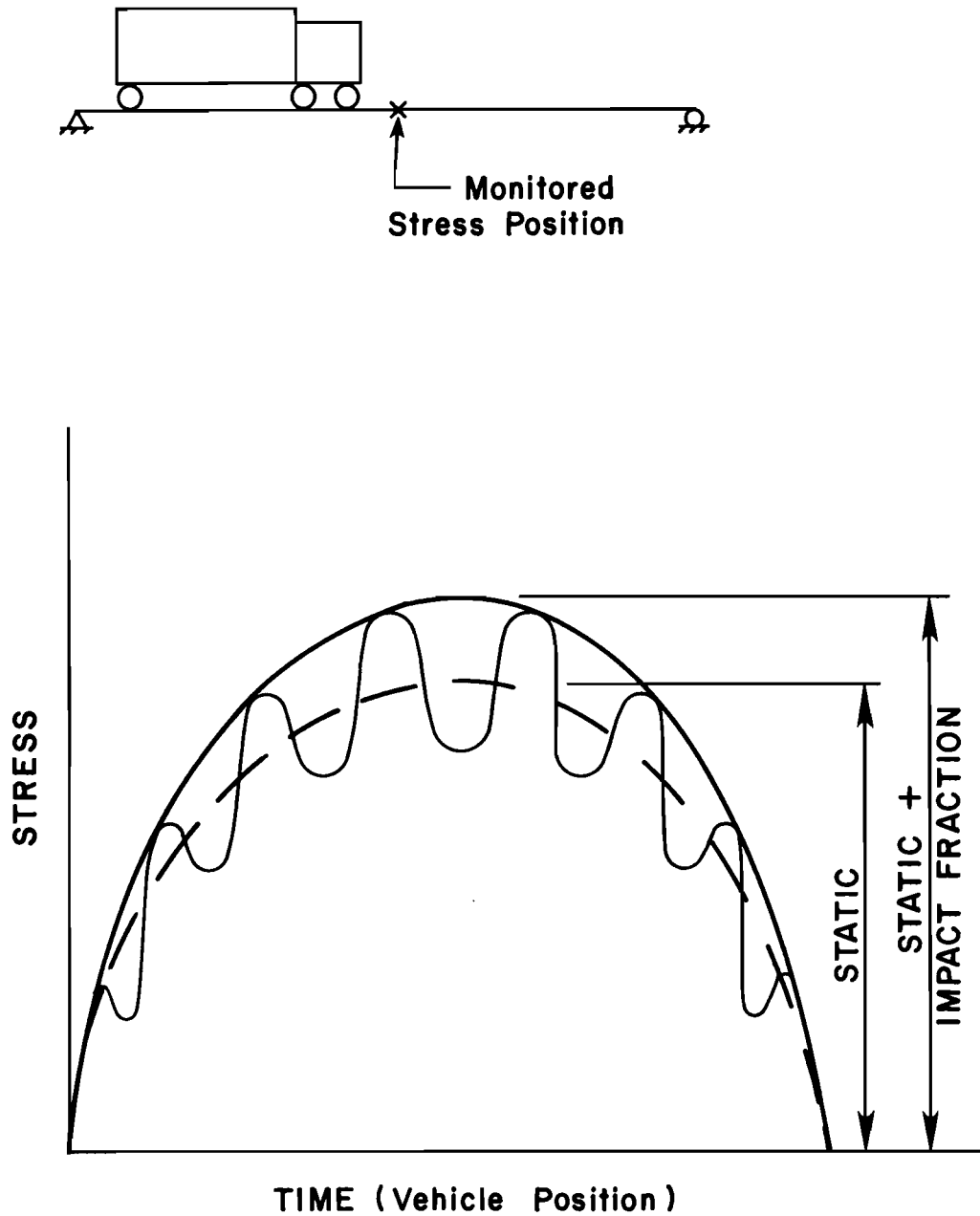
Fig. 1.2 Plot showing use of impact fraction to account for

increase in static stress due to dynamic loading

application of linear cumulative damage to complex waveforms as exhib-
ited by a bridge in the field is uncertain. In addition, there are var-
ious methods of counting stress cycles. The new British bridge fatigue
design rules employ reservoir counting.[4] However, no experimental
verification of this stress counting method currently exists. Most of
the experimental work done in variable amplitude testing has been per-
formed on waveforms with constant minimum stress. The stress cycles in
these waveforms are well defined, but the damage caused by these wave-
forms may not be similar to the damage associated with bridge stress
waveforms.

1.2 OBJECTIVE

The primary objective of this study is to determine exper-
imentally the influence that superimposed high frequency/low stress
cycles have on the fatigue life of low frequency/high amplitude stress
cycles. Tests were conducted on welded steel tees loaded in bending.
The validity of using an effective stress approach based on reservoir
counting and linear cumulative damage rule to predict fatigue life was
investigated. Other fatigue life prediction methods were examined. The
findings of these tests will aid in linking constant amplitude data to
variable amplitude data measured in the field.

This is the first part of a larger study addressing the problem
of how much damage occurs due to the additional stress cycles associated
with truck loading. An effective stress approach will be employed to
account for this additional damage.

1.3 CUMULATIVE DAMAGE

Cumulative damage rules account for the damage effect of stress cycles by using known constant amplitude fatigue behavior. This can be demonstrated by looking at the S-N curve obtained from constant amplitude fatigue tests as shown in Fig. 1.3. For each level of stress, S_i, there is an associated failure life, N_i. The damage can be expressed as a fractional quantity of the number of cycles to failure, n_i. This fractional damage, D_i, due to "S_i" which occurs "n_i" cycles is as follows:

$$D_i = \frac{n_i}{N_i} \tag{1.2}$$

When $D_i = 1$, failure is predicted since $n_i = N_i$.

If we assume that the damage effect of each stress range in a complex waveform is independent of one another, a generalized expression for total damage, D, can be expressed in terms of D_i as follows:

$$D = \sum_i D_i \tag{1.3}$$

As before, failure is predicted when $D = 1$ or more commonly expressed:

$$\sum_i \frac{n_i}{N_i} = 1 \tag{1.4}$$

This linear damage accumulation hypothesis is referred to as the Palmgren-Miner hypothesis or Miner's rule. Miner's rule is well suited for determining the percent of fatigue life used. In order to predict failure life, the application of Miner's rule is cumbersome. Usually an effective stress approach is used in predicting failure life.
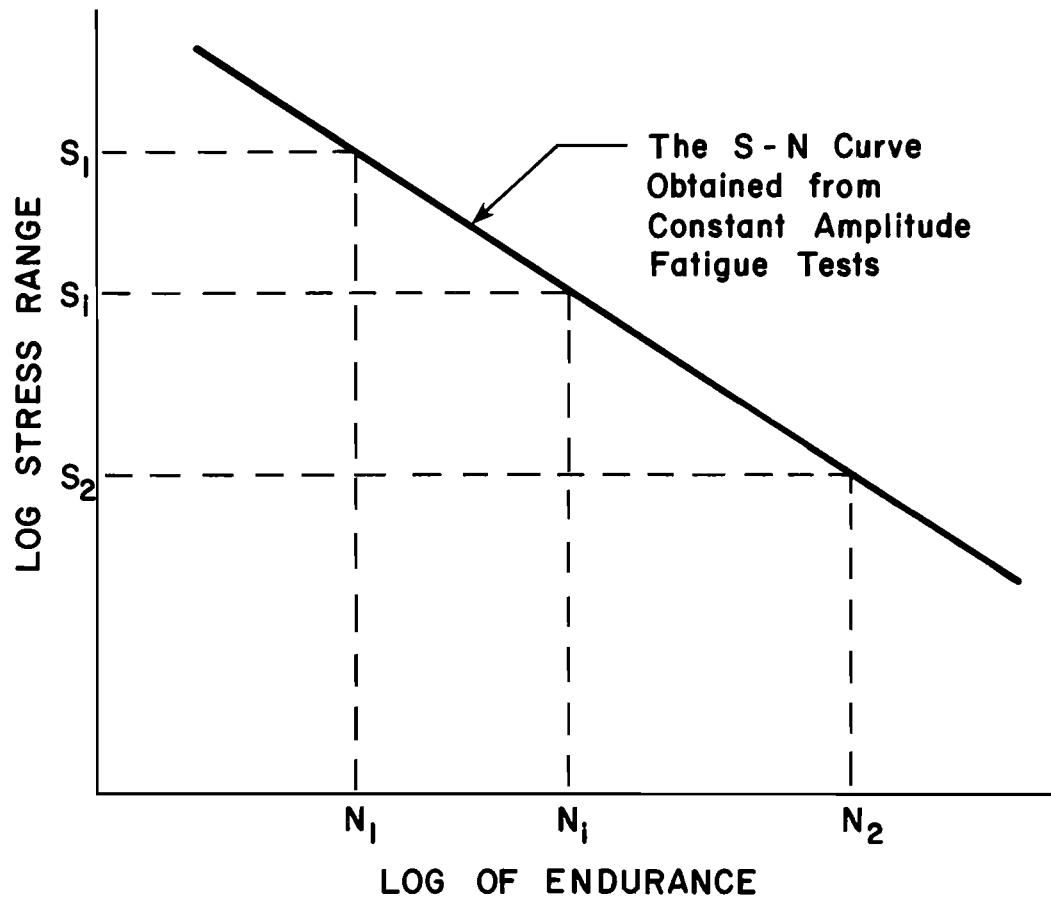
Fig. 1.3 Prediction of cycles to failure from S-N curve based

on constant amplitude fatigue tests

1.4 EFFECTIVE STRESS

An effective stress, S_{re}, is a constant amplitude stress reproducing fatigue life associated with some stress history. An expression for S_{re} can be developed from the equation of an S-N curve and the application of Miner's rule. In general, the equation of an S-N curve is given by

$$\text{Log } N_i = A - m \text{ Log } S_i \tag{1.5}$$

or

$$N_i = 10^A S_i^{-m} \tag{1.6}$$

where "A" and "m" are regression coefficients obtained from a least squares best fit. Substituting N_i from eqn. 1.6 into eqn. 1.4, Miner's rule, gives:

$$\sum_i \frac{n_i}{10^A S_i^{-m}} = 1.0 \tag{1.7}$$

Using eqn. 1.6, the fatigue life N is written in terms of S_{re} as follows:

$$N = 10^A S_{re}^{-m} \tag{1.8}$$

or

$$\frac{N \, S_{re}^m}{10^A} = 1.0 \tag{1.9}$$

Equating eqn. 1.7 with eqn. 1.9 and solving for S_{re} gives

$$S_{re} = \left[\sum_i \frac{n_i S_i^m}{N} \right]^{1/m} \tag{1.10}$$

or

$$S_{re} = \left[\sum_i \gamma_i S_i^m \right]^{1/m} \tag{1.11}$$

where γ_i is the relative occurrence of n_i with respect to the total number of cycles N.

In general, welded bridge details have a slope of 3 on a log-log S-N curve. In constant amplitude testing done by the U. S. Steel Corporation[10], two details, a cover-plated beam and a welded beam, had slopes of 2.982 and 3.296 respectively. Variable amplitude tests were conducted on these two details using a Rayleigh distribution of stress ranges where every stress range had the same minimum stress level. Different ordering of the stresses did not cause an apparent difference in fatigue life. The variable amplitude data was plotted at effective stress values using m equal to 2 (root mean squared - rms) and 3 (root mean cubed - rmc) in eqn. 1.11. In these tests, the effective stress plotted at either the value of S_{rms} or S_{rmc} fell within a scatter band bounded by the 95 percent confidence limits of the constant amplitude data. Since the fatigue lives at S_{rms} led to a slightly better fit of the constant amplitude S-N curve than did S_{rmc}, they concluded that the rms value is more accurate than the rmc value.

In general, S_{rms} may not lead to a good fatigue life prediction. This becomes apparent from the following fatigue life prediction example using both an rms and an rmc calculated effective stress range. The S-N curve and stress loading histogram for this example are shown in Fig. 1.4. Note that the slope of the S-N curve has purposely been set to 3 to demonstrate that the fatigue life prediction based on S_{rmc} would give a Miner's sum $= 1$. Based on the stress histogram shown in Fig. 1.4:

$$S_{rmc} = [0.8(10)^3 + 0.2(25)^3]^{1/3}$$

$$= 15.77$$

and
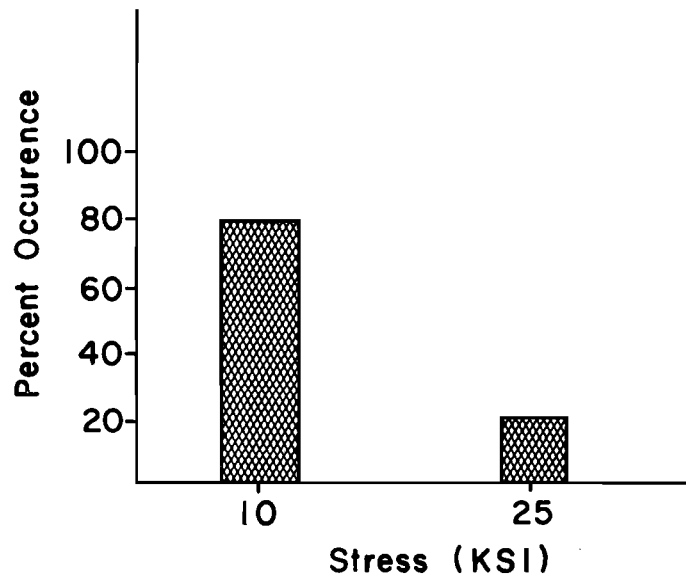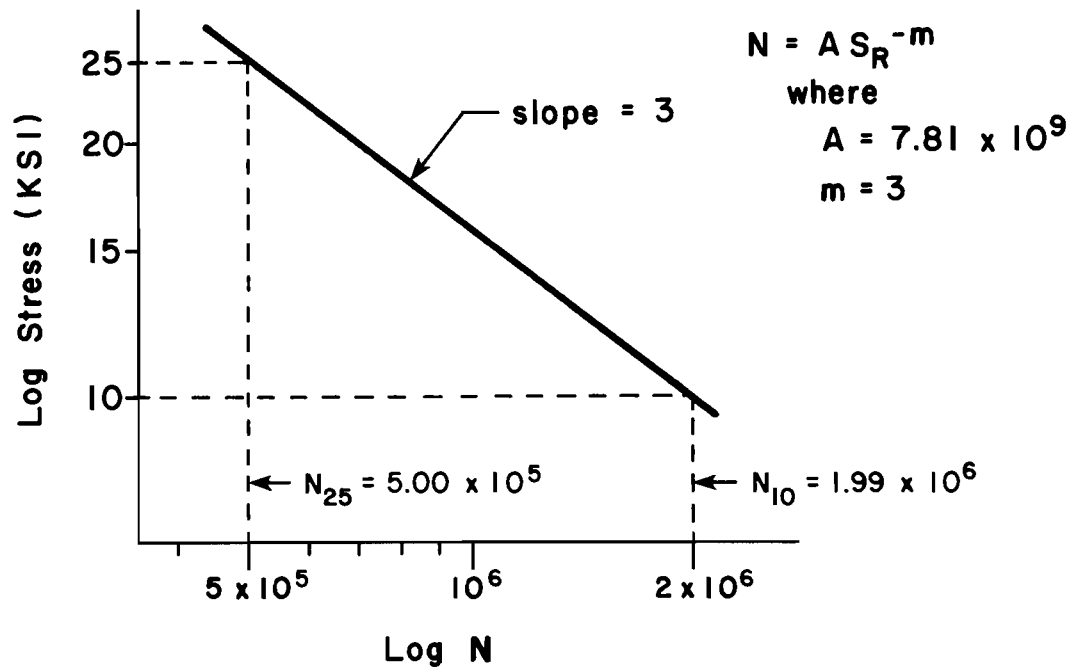
Fig. 1.4   Example S-N curve and stress loading histogram

$$S_{rms} = [0.8(10)^2 + 0.2(25)^2]^{1/2}$$
$$= 14.32$$

The corresponding cycles to failure are given by

$$N_{rmc} = 7.8125 \times 10^9 (15.77)^{-3}$$
$$= 1,990,511 \text{ cycles}$$

and

$$N_{rms} = 7.8125 \times 10^9 (14.32)^{-3}$$
$$= 2,661,601 \text{ cycles}$$

The associated cumulative damage becomes

$$\Sigma \frac{n}{N} = \frac{n_{25}}{N_{25}} + \frac{n_{10}}{N_{10}}$$

$$\Sigma \frac{n}{N} \text{ for rmc} = \frac{0.2(1,990,511)}{500,000} + \frac{0.8(1,990,511)}{7,812,500}$$
$$= 0.7962 + 0.2038$$
$$= 1.0000$$

$$\Sigma \frac{n}{N} \text{ for rms} = \frac{0.2(2,661,601)}{500,000} + \frac{0.8(2,661,601)}{7,812,500}$$
$$= 1.0646 + 0.2725$$
$$= 1.3372$$

Note: 0.7962 and 1.0646 are the damages associated with the 25 ksi stress.

The results of this particular example show three interesting points. 1) The rmc approach gives a cumulative damage of 1.00 which follows the linear cumulative damage law. 2) The rms approach gives a linear cumulative damage of 1.34. 3) The number of 25 ksi stress cycles required using the root mean squared approach is greater than the

number of 25 ksi stress cycles needed for failure in a constant amplitude test. The coefficient in the example is seen to be greater than 1. In other words, the effective stress based on an rms approach indicates 532,320 cycles of 25 ksi stress range would occur before failure, although the S-N curve predicts 500,000 cycles of 25 ksi stress range to failure. If this is true, the smaller cycles at 10 ksi increase the fatigue life. This is contrary to what experimental results in the present study would indicate. Had the value of "m" been equal to the slope of the log-log S-N curve, the smaller cycles of stress would not have increased the number of 25 ksi stresses needed to failure above N_c, the number of constant amplitude cycles to failure. A proof follows in Appendix I. Thus, the effective stress calculations, where effective stress range, S_{re}, is defined as in eqn. 1.11, should be performed with a value of m set as close to the slope of a representative log-log S-N curve. Again, the rmc approach is expected to give good fatigue prediction as welded details have S-N curve slopes of about 3.

1.4 RESERVOIR COUNTING

Before an effective stress concept can be employed, the stresses from a stress history must be determined. In a stress history as previously shown in Fig. 1.1 for the truck load moving at 50 mph, it is not obvious what constitutes a stress cycle or how stress cycles should be counted. The reservoir (or rainflow) counting method is generally used in counting stresses. The reservoir counting method is considered the best method for predicting fatigue life.[2] This is because the

reservoir counting method identifies major stress range cycles associated with low frequency components (i.e. as may result from a slowly varying mean stress). It does this while simultaneously identifying smaller high frequency stresses. The reservoir method is particularly attractive because it is easy to apply and makes complete use of the stress history.

The easiest way to illustrate the reservoir counting method is to consider a stress history, like the one shown in Fig. 1.5, filled with water. In order to determine the stresses, the reservoir is drained by letting the water out at the minimum peak stress values. The water is first drained at the lowest peak stress value, point 6 in Fig. 1.5. Then the water is drained at the next lowest peak stress value and so on until all the water has been drained. Each minimum peak designates a stress cycle. The number of stress cycles in a stress history can be determined by counting the number of times a minimum peak stress occurs. The corresponding height of the water drained at each minimum peak stress constitutes a stress range as shown by cross hatching in Fig. 1.5. From these stresses, an effective stress can be calculated.

1.5 TENSILE COUNTING METHOD

Since fatigue crack growth occurs during the tensile portion of a stress range, an alternate method referred to as the tensile counting method can be employed. The tensile counting method counts only the stress ranges as they are confronted. Using the stress waveform shown in Fig. 1.6, the tensile counted stresses are denoted z'. The effective
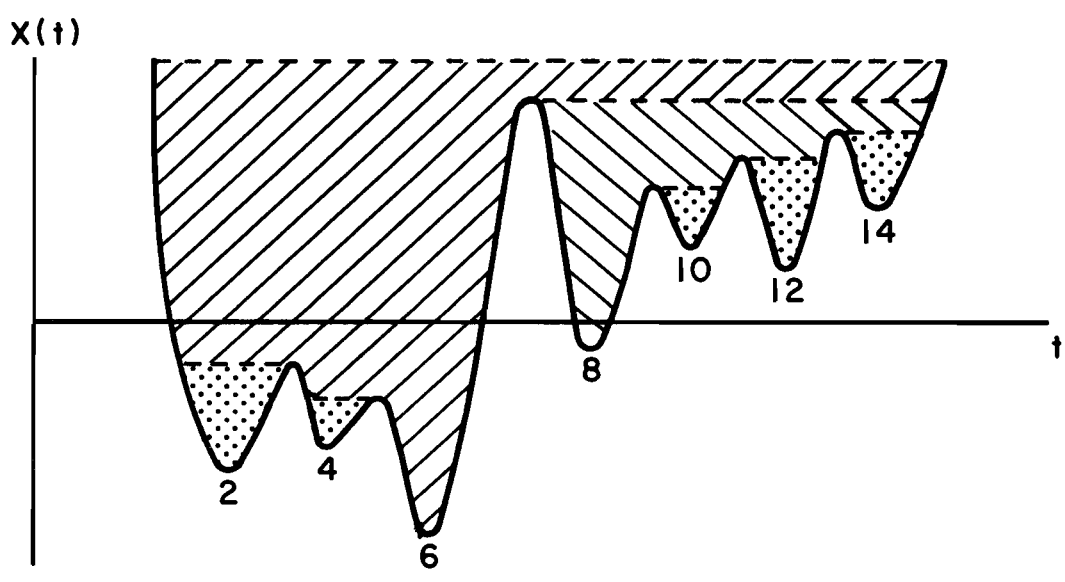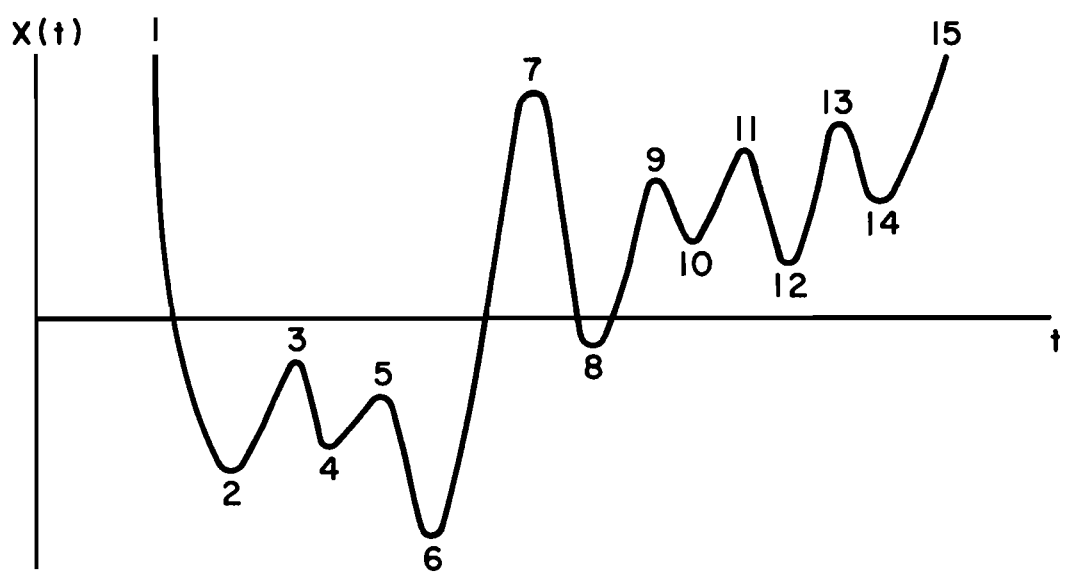
Fig. 1.5 Applying reservoir counting to a stress history
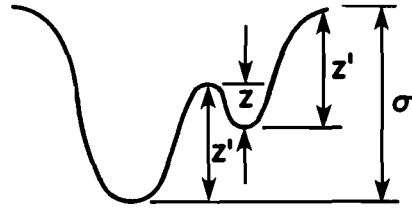
Fig. 1.6 Constant amplitude wave with a single stress excursion z
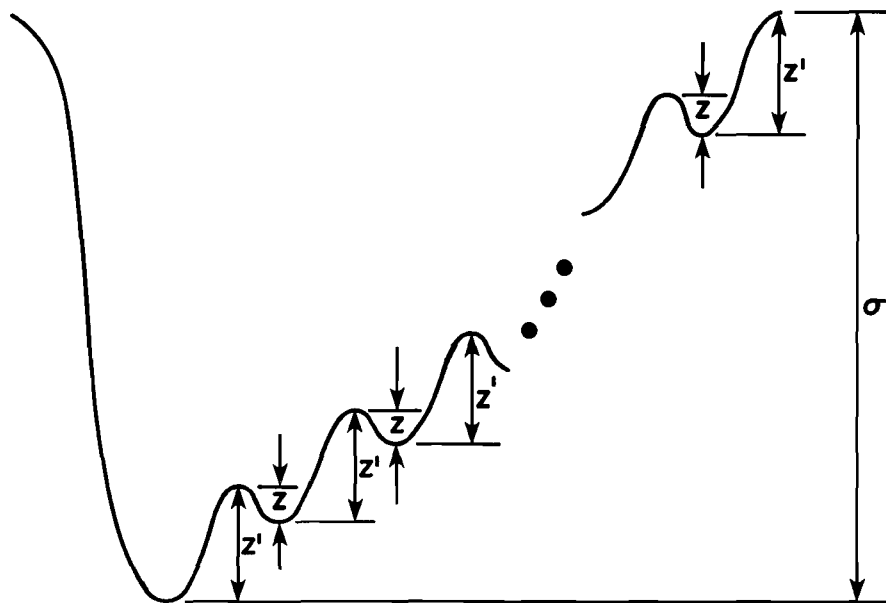
Fig. 1.7 Constant amplitude wave with "v" excursions of stress z

stress range using tensile counting with designation S_{rt} would be:

$$S_{rt} = z' \qquad \text{where } z' = (\sigma + z)/2 \qquad (1.12)$$

The corresponding effective stress range using reservoir counting with designation S_{rr} would be:

$$S_{rr} = \left[\frac{1}{2}\sigma^m + \frac{1}{2}z^m\right]^{1/m} \qquad (1.13)$$

Note that 2 cycles of stress are counted by both counting methods for each occurrence of the waveform shown in Fig. 1.6. In general, both counting methods produce the same number of stress cycles.

It is of interest to see which of the two counting methods above, if any lends itself to a more accurate prediction of fatigue life. For the waveform of Fig. 1.7, both of these counting methods give "v" cycles of stress for each occurrence of the stress waveform. Thus, the fatigue life prediction based on either of these counting methods can be directly related by viewing the ratio of the effective stresses. A higher effective stress would yield a more conservative prediction of fatigue life. It can be shown that for a waveform of Fig. 1.7 with "v" occurrences of single stress excursion size "z", that $S_{rr} > S_{rt}$ if $m > 1$. S_{rr} and S_{rt} are expressed as:

$$S_{rr} = \left[\frac{1}{1 + v}\sigma^m + \frac{v}{1 + v}z^m\right]^{1/m} \qquad (1.14)$$

and

$$S_{rt} = z' \qquad \text{where } z' = (\sigma + vz)/(1 + v) \qquad (1.15)$$

The ratio of S_{rr} to S_{rt} can be expressed using eqns. 1.14 and 1.15 as

$$\frac{S_{rr}}{S_{rt}} = \frac{\left[\dfrac{1}{1 + v}\sigma^m + \dfrac{v}{1 + v}z^m\right]^{1/m}}{\left[\dfrac{\sigma + vz}{v + 1}\right]} \qquad (1.16)$$

Multiplying the numerator and denominator by $1/\sigma$, substituting p for

z/σ, and re-arranging terms gives:

$$\frac{S_{rr}}{S_{rt}} = \frac{(1 + v)^{m-1}(1 + vp^m)^{1/m}}{1 + vp} \tag{1.17}$$

With p equal to 1, S_{rr}/S_{rt} reduces to 1. Assuming that $S_{rr}/S_{rt} > 1$, we can say that $\ell n(S_{rr}/S_{rt}) > 0$. Defining $F = \ell n(S_{rr}/S_{rt})$, then:

$$F = \ell n\left[\frac{(1 + v)^{m-1}(1 + vp^m)^{1/m}}{(1 + vp)}\right] \tag{1.18}$$

or

$$F = \frac{m - 1}{m}\ell n(1 + v) + \frac{1}{m}\ell n(1 + vp^m) - \ell n(1 + vp) \tag{1.19}$$

From this follows:

$$\frac{\partial F}{\partial p} = \frac{vp^{m-1}}{1 + vp^m} - \frac{v}{1 + vp} \tag{1.20}$$

To find the location of minimum or maximum p value, set $\partial F/\partial p = 0$. From eqn. 1.20

$$1 + vp^m = (1 + vp)p^{m-1} \tag{1.21}$$

or

$$1 = p^{m-1} \tag{1.22}$$

For m > 1, F is a minimum or maximum when p = 1. Thus, in order to determine if F is a minimum or maximum when p = 1, find $\partial^2 F/\partial p^2$. It can be shown that

$$\frac{\partial^2 F}{\partial p^2} = 0 \qquad \text{when } p = 1 \tag{1.23}$$

and

$$\frac{\partial^2 F}{\partial p^2} > 0 \qquad \text{when } 0 \le p < 1 \text{ and } m > 1 \tag{1.24}$$

This implies that F is a minimum which verifies our initial assumption that $S_{rr}/S_{rt} > 1$. Thus, for constant amplitude waveforms with constant size excursions "z", a more conservative fatigue life prediction will

result from effective stresses based on reservoir counting rather than on tensile counting.

1.6 GURNEY'S EFFECTIVE STRESS

Another alternative for possible consideration in effective stress determination is stress interaction effects. Stress interaction means that the damage effect of one stress range can influence the damage effect of another stress range. Stress interaction is very difficult to model. An easy way to handle stress interaction is to relate the damage associated with complex waveforms to upper and lower limit constant amplitude waveforms as Gurney did in ref. 4. Gurney took a lower limit - upper limit approach in obtaining interaction effects between various levels of stress range. An upper and lower limit can be established by examining the waveform in Fig.1.8. This waveform is a simple sine function of amplitude σ with a single excursion of size z. By upper limit, we mean that the effective damage caused by the waveform can not be greater than the same waveform with stress excursion size $z = \sigma$. By the same token, the lower limit approach implies that the effective damage caused by the waveform can not be less than the same waveform with stress excursion size $z = 0$. As shown in Fig. 1.8, the waveform degenerates into constant amplitude waves at upper and lower limits. Gurney performed fatigue tests with simple waveforms like the one shown in Fig. 1.8. He observed a linear relationship between p, the ratio of the magnitude of the stress excursion z to the stress range σ, and log N, where "N" is the number of times the stress σ occurs. In
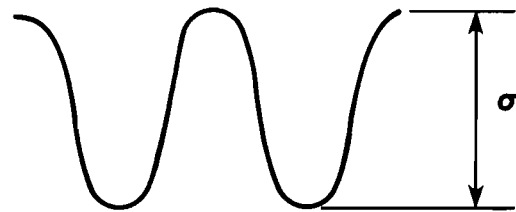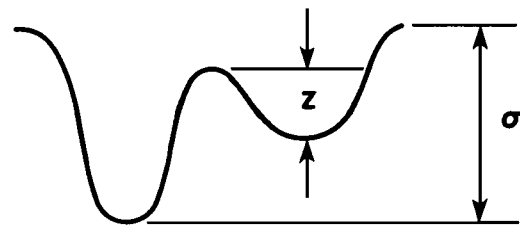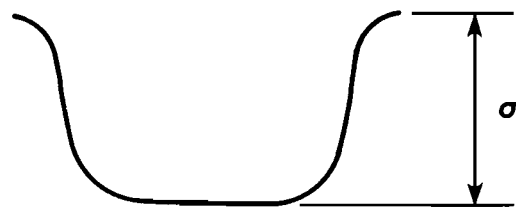
Fig. 1.8   Single constant amplitude wave with single

stress excursion z

mathematical form, this relationship becomes:

$$\text{Log } N \propto p \qquad \text{where } p = z/\sigma \tag{1.25}$$

A generalized equation using eqn. 1.25 can be written which satisfies upper and lower limits as follows:

$$\text{Log } N = \text{Log } N_c - p \text{ Log}(1 + v) \tag{1.26}$$

or

$$N = N_c(1 + v)^{-p} \tag{1.27}$$

where "v" is the number of excursions of size "z" and "N_c" is the number of constant amplitude cycles with amplitude "σ" to cause failure. At lower limit, z = 0, the predicted life becomes $N_c/(1 + v)$ as the total number of peaks in a complex waveform is "1 + v".

The number of cycles, N_t, of σ plus every cycle of excursion size z, based on an effective stress approach is as follows:

$$N_t = A \ S_{rg}^{-m} \tag{1.28}$$

or

$$S_{rg} = (A/N_t)^{1/m} \tag{1.29}$$

where S_{rg} is the effective stress based on Gurney's cycle life interaction expression, eqn 1.27. Substituting $(1 + v)N = N_t$ and eqn. 1.27 for N gives

$$S_{rg} = (A/[N_c(1 + v)^{1-p}])^{1/m} \tag{1.30}$$

Substituting $A\sigma^{-m} = N_c$ and cancelling terms gives

$$S_{rg} = \sigma(1 + v)^{(p-1)/m} \tag{1.31}$$

S_{rr}, effective stress based on reservoir counting of waveforms with single size excursion z, is given by

$$S_{rr} = \left[\frac{1}{1 + v}\sigma^m + \frac{v}{1 + v}z^m\right]^{1/m} \tag{1.32}$$

Substituting $p\sigma = z$ into eqn. 1.32 and dividing S_{rg} by S_{rr} gives

$$\frac{S_{rg}}{S_{rr}} = \frac{\sigma(1 + v)^{(p-1)/m}}{\frac{1}{1 + v}\sigma^m + \frac{v}{1 + v}(p\sigma)^m} \qquad (1.33)$$

Factoring and substituting z/σ for p, and cancelling terms results in

$$\frac{S_{rg}}{S_{rr}} = \frac{(1 + v)^{z/\sigma}}{1 + v(z/\sigma)^m} \qquad (1.34)$$

This is a simple expression for waveforms with constant size z in terms of only z/σ, v, and m.

Using m = 3, a plot of S_{rg}/S_{rr} vs. z/σ is shown in Fig. 1.9 for v excursions of stress size z. From this plot, it is evident that with just a single stress excursion of z/σ = 0.25 that S_{rr} is 5% lower than S_{rg}. It is possible for these effective stresses to differ by as much as 18%, which translates into a fatigue prediction difference of 39% for this example. Note that S_{rg}/S_{rr} are a maximum at z/σ between 0.3 to 0.4 when v is 5 to 15.

1.7 TEST APPROACH

The testing performed in this study was either constant amplitude, CA, or superimposed sine, SS. Superimposed sine tests involved taking two separately generated sine functions and summing the signals together. A resulting general waveform is shown in Fig. 1.10. Variations of this waveform could be generated by adjusting the relative magnitude and the relative frequency of the sine waves.

Once the S-N curve was established from constant amplitude tests, a series of superimposed sine tests were conducted. From these preliminary SS tests, two different experiments were initiated.
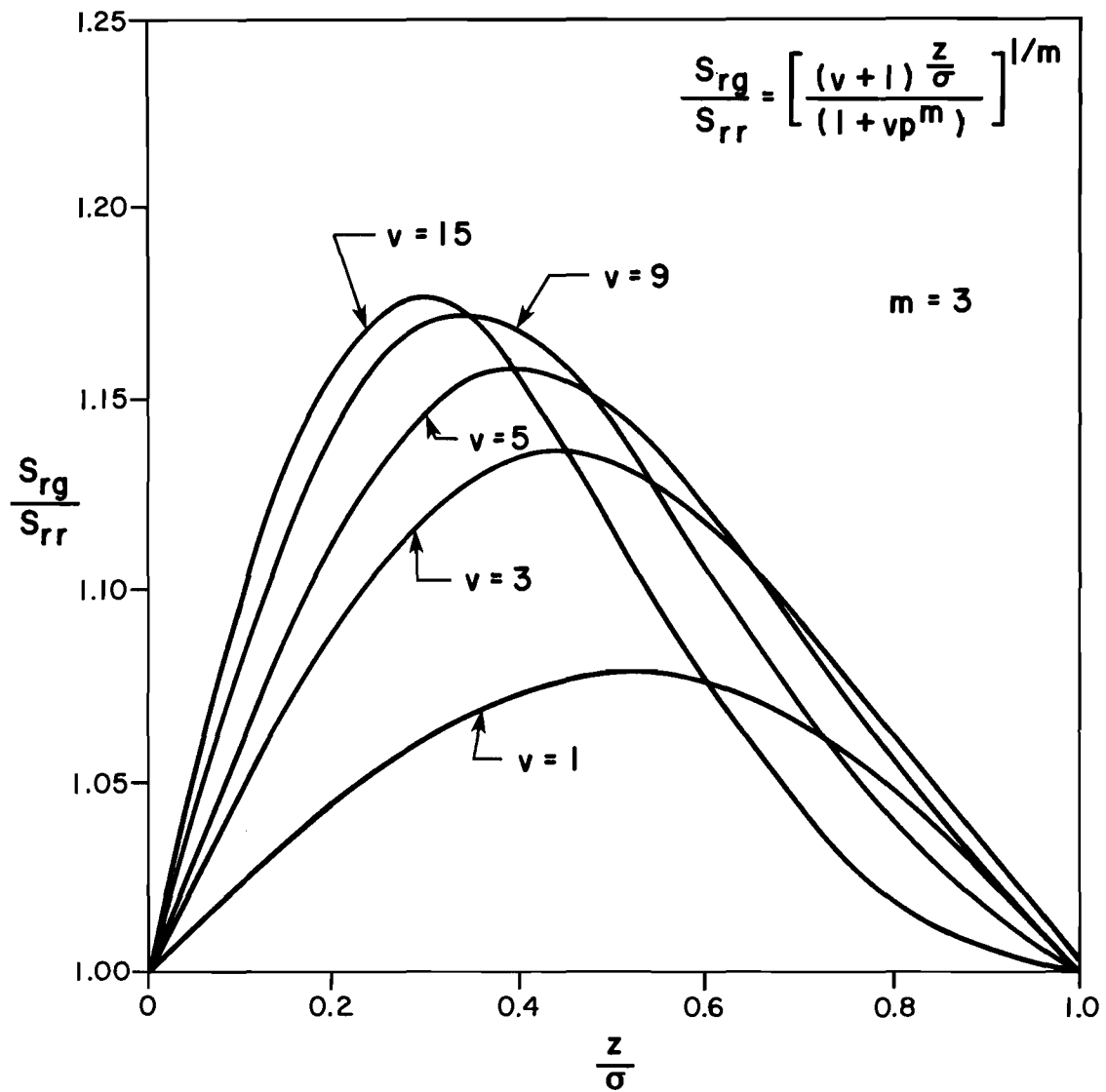
Fig. 1.9 S_{rg}/S_{rr} vs. z/~ at m = 3 for single
size excursion stresses
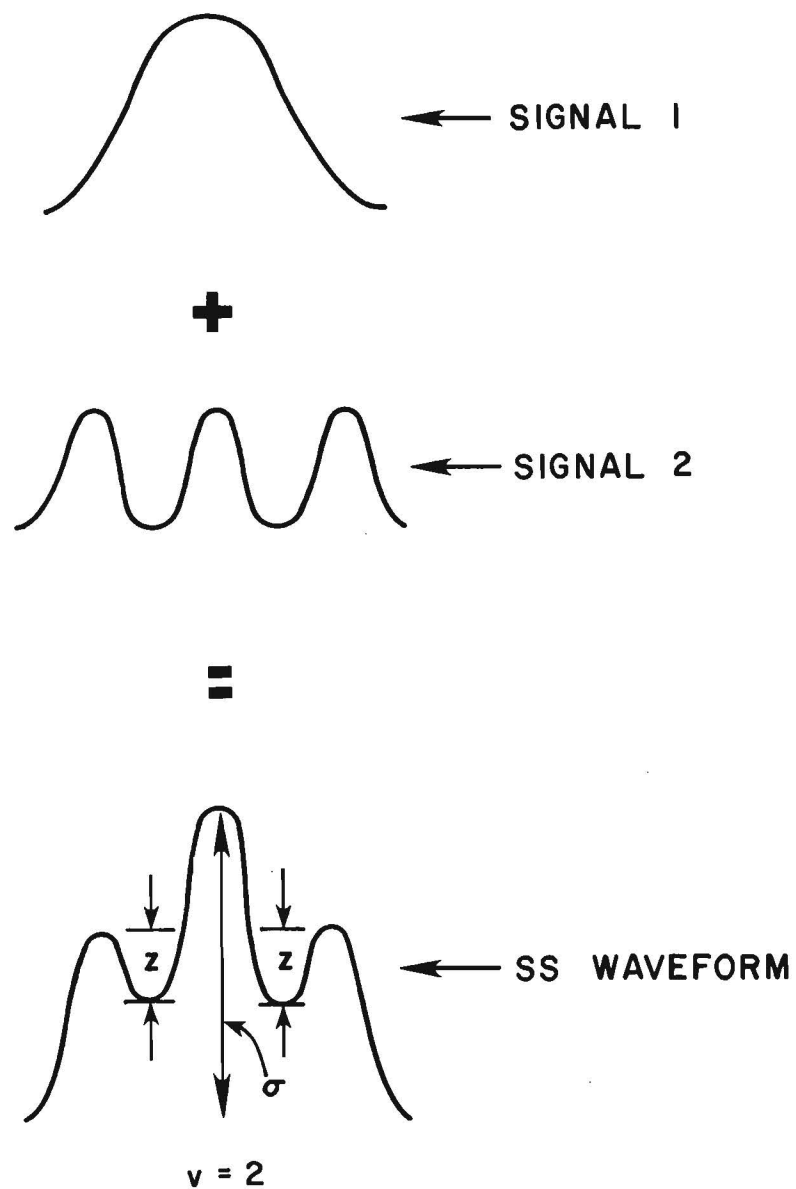
Fig. 1.10 Superimposed sine waveform from two sine waves

The first experiment was performed to examine the ability of an effective stress range based on reservoir counting and linear cumulative damage rule to predict fatigue life. Waveforms were chosen to produce a constant effective stress range, 18 ksi. Since little CA data was available at the time the experiment was begun, effective stresses were determined on the basis of a root mean cubed approach. The minor stress excursions, z, were kept at an average of 15 ksi with the major stress, σ, being varied between 25 ksi and 35 ksi. The ratio of major stress occurrence to minor stress occurrence was varied between 1/5 and 1/16 for the respective tests as shown in Fig. 1.11.

The second experiment was performed to determine the damaging effect of small stresses. This was achieved by fixing the major stress range at 30 ksi and the cyclic ratio of major and minor occurrences at 1/10. The minor stress was varied between 20 ksi and 10 ksi. This is shown in Fig. 1.12.

Case	v + l	σ
1	10	30
2	16	35
3	5	25

z = 15 ksi
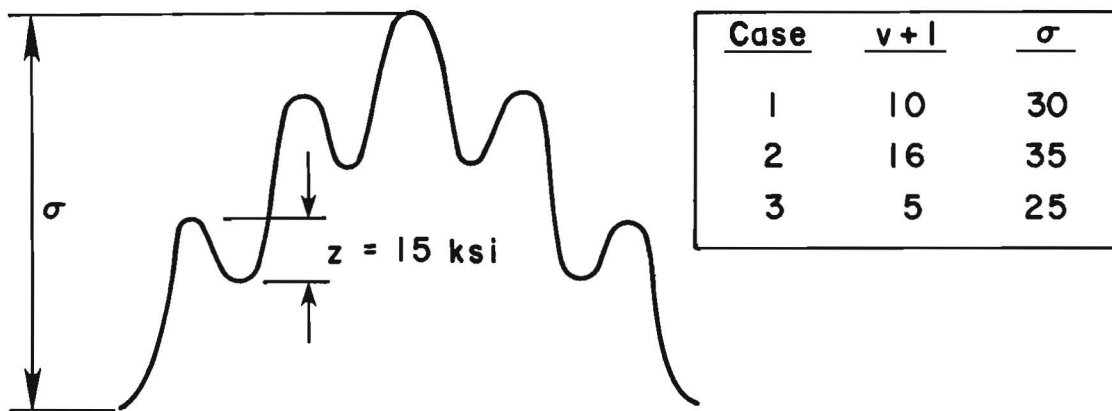
Fig. 1.11   Experiment 1:   SS testing

Case	z
1	20
2	14
3	10

σ = 30 ksi

v + l = 10
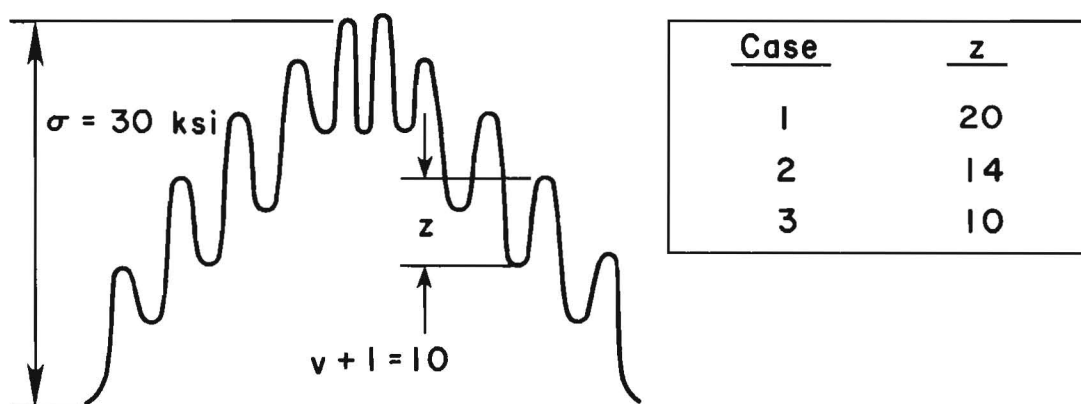
Fig. 1.12   Experiment 2:   SS testing

CHAPTER 2: TESTING PROGRAM

2.1 SPECIMEN DESIGN

The tests were conducted on welded steel tee sections loaded in cantilever bending. This specimen could be easily fabricated and proved to be an attractive solution to the overall experiment design. The primary reason for selecting this specimen was the ability to test at high frequency. This was critical in reducing testing time. To ensure that failure occurred along the weld toe (not in the weld root), the end of the stem plate to be welded was beveled to produce a partial penetration. The weld was sized in accordance with recommendations made by Ouchida & Nishioka [8]. Specimen geometry is shown in Fig. 2.1.

All steel used was from the same heat of steel. The mill test report shows that this steel meets the chemical and mechanical requirements as set forth by ASTM Type 1 A572-50 grade steel. A summary of the mill test report is shown in Table 2.1. The chemistry of a sample was checked and shown as the laboratory results in Table 2.1.

2.2 SPECIMEN FABRICATION

This weldment was made from 2 plates of 1 inch thick A572-50 grade steel. These plates measured 13"x3'-6" and 8"x3'-6" respectively. A 5/16" bevel was flame cut along each side of one of the

25

13"

4"

A

A

Detail 1

D = $\frac{13"}{16}$ (TYP.)

8"

1.5"

5"

1.5"

View A-A

1"

₵

45°

Note:
Symmetric
about ₵

$\frac{5}{8}$" $\frac{5}{16}$"

1"

Detail 1
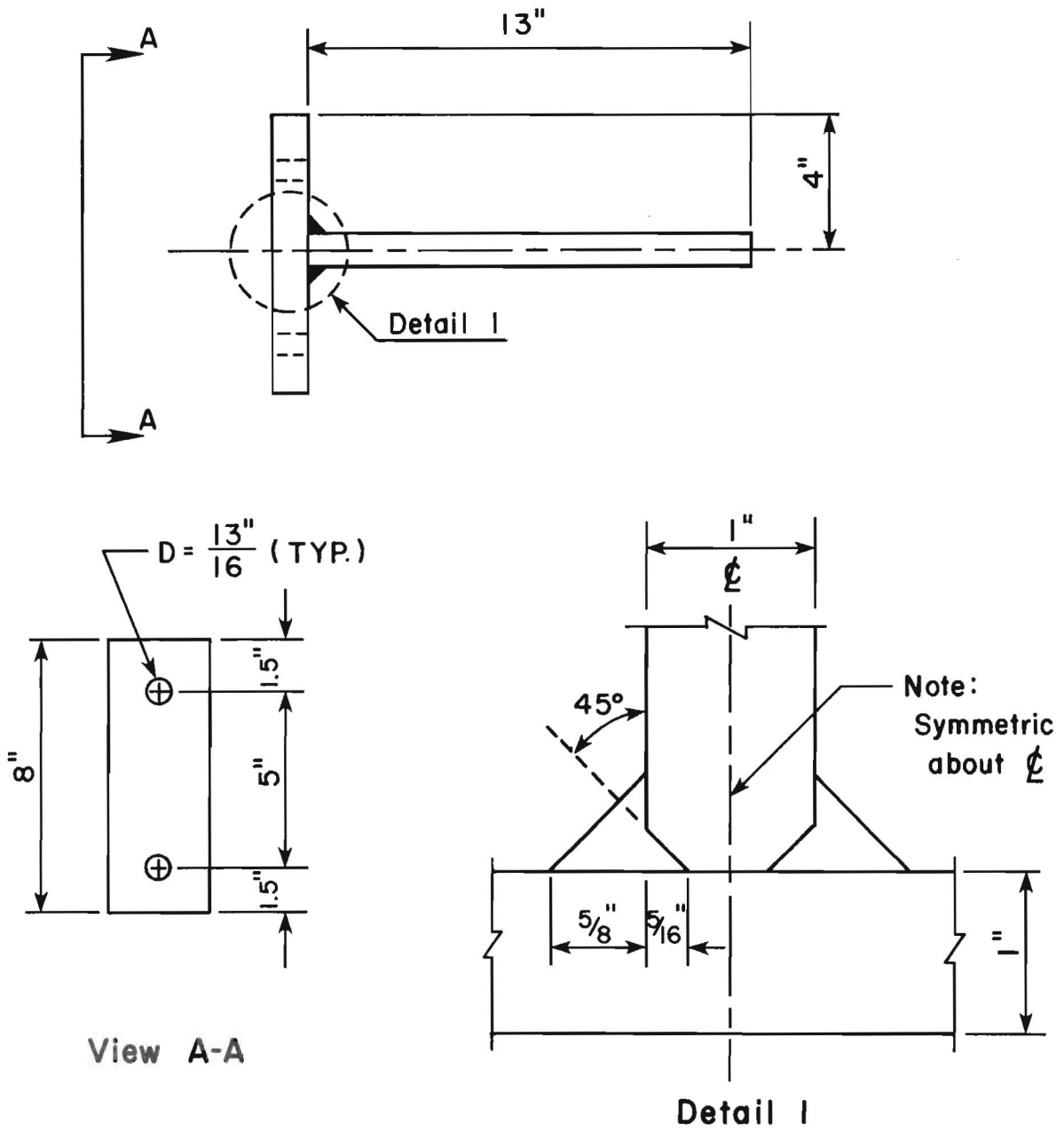
Fig. 2.1 Test specimen geometry

TABLE 2.1 MILL TEST REPORT

Steel Grade: A572-50

Chemical Composition

	C	Si	Mn	P	S	Cr	Ni	Mo	V	Cu	Nb
Mill Ladle Analysis (%):	0.19	0.23	1.12	0.019	0.019				0.007		0.030
Mill Product Analysis (%):	0.18	0.22	1.09	0.018	0.016						0.029
[1]Laboratory Analysis (%):	0.17	0.23	1.11	0.013	0.022	0.18	0.02	0.01		0.01	0.027
ASTM Heat Analysis (Type 1) Requirements	0.23 max	0.40 max	0.80-1.65	0.04 max	0.05 max						0.005-0.05

[1]Chicago Spectro Service Laboratory, Inc.

Mechanical Strength (Mill Test Results)

	Tensile Test	ASTM Required
Yield Point:	58 ksi	50 ksi
Tensile Strength:	81.2 ksi	65 ksi

long edges of the 13"x3'-6" plate. This large plate was placed perpendicular to the 8"x3'-6" plate with the beveled edge centered on the 8" side. The plates were tack welded to hold the plates in position.

A series of 18 weld passes, 9 for each weld, were made alternately on each side using a manual SMAW process. The first weld pass on each side of the long edge was made using a 3/32"-7018 low hydrogen rod at 26 volts DC and 120 amps. The remaining eight passes on a side were made using an 1/8"-7018 low hydrogen rod at 27 volts DC and 150 amps. The welding sequence is shown in Fig. 2.2.

After the welding was finished, the weldment was marked for identification by painting an edge with a stripe so the origin of each specimen could be established. Since only one side was painted, the same side weld toe could be identified and tested for a given weldment.

Next, the specimens were cut out of the weldment using a machine saw. First, a 1/2" slice was cut away from each end of the weldment to remove the beginning and end of the weld. Then thirteen - 3" wide specimens were cut out. Following the cutting, each specimen had two - 13/16" diameter holes drilled 5" apart in the flange of the tee. The holes were used to bolt the specimen to the test frame.

2.3 TEST SETUP

The test arrangement shown in Fig. 2.3 is a closed loop hydraulic fatigue testing system comprised of three major components: 1) the testing frame, 2) the hydraulic system, and 3) the electronic console.

The test specimen is bolted to the inside vertical face of the

Fig. 2.2 Welding procedure
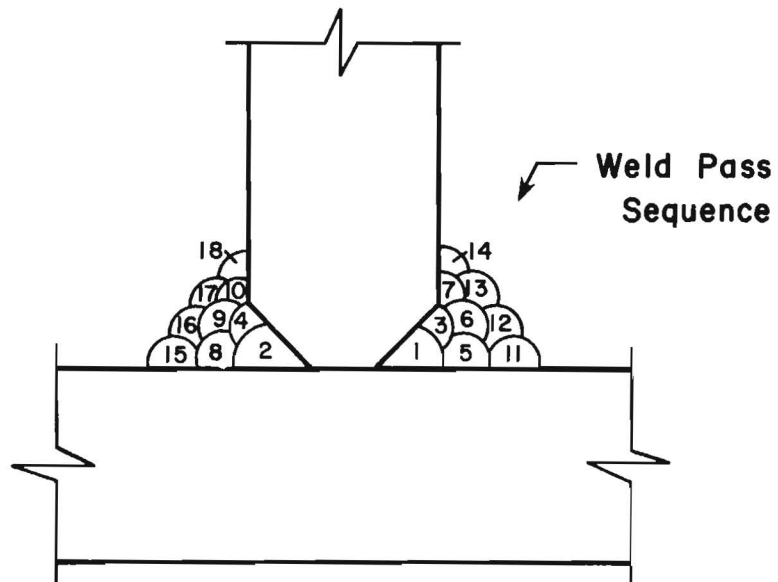
Weld Pass No.	Electrode	Current, Amps	Voltage, Volts DC
1 & 2	3/32"-7018 Low Hydrogen	100	26
3 - 18	1/8"-7018 Low Hydrogen	150	27
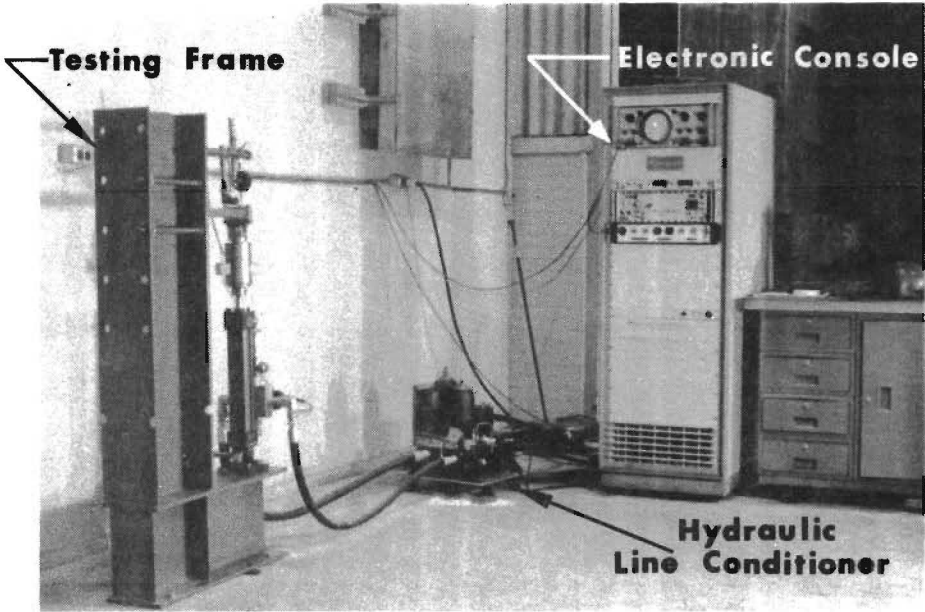
Fig. 2.3 Test arrangement

"L" shaped test frame as shown in Fig. 2.4. The knife edge loading system is shown in Fig. 2.5. A 5 kip load cell is connected between the hydraulic ram and the knife edge.

The hydraulic system provides a constant 3000 psi pressure. The servo valve mounted on the loading ram directs the hydraulic flow to the top or bottom of the ram in response to commands from the servo controller. The hydraulic ram always applies load in one direction, i.e. upwards into the specimen.

The programmed waveforms were developed from function generator signals. Unlike CA testing where one sine wave signal is needed, two function generators were used together to produce the superimposed sine testing experiments. The function generator signals were run at different relative frequencies and different relative amplitudes. The two signals were superimposed by the use of a summing junction circuit.

2.4 TESTING PROCEDURE

The programmed loads were determined from the desired nominal bending stress (σ) in the extreme tensile fiber of the test specimen at the weld toe as follows:

$$P = \frac{\sigma \, S}{L}$$

where "S" is the section modulus and "L" is the moment arm (distance from knife edge to weld toe). One measurement of the specimen width and four of the specimen thickness were made. The specimen's width was measured at the weld toe. The average of the measured dimensions were used

Fig. 2.4   Test frame

Fig. 2.5 Knife edge loading system

to calculate the section modulus of the specimen. Thickness was determined by averaging the measured plate thickness at four locations along the weld toe. The moment arm was computed from t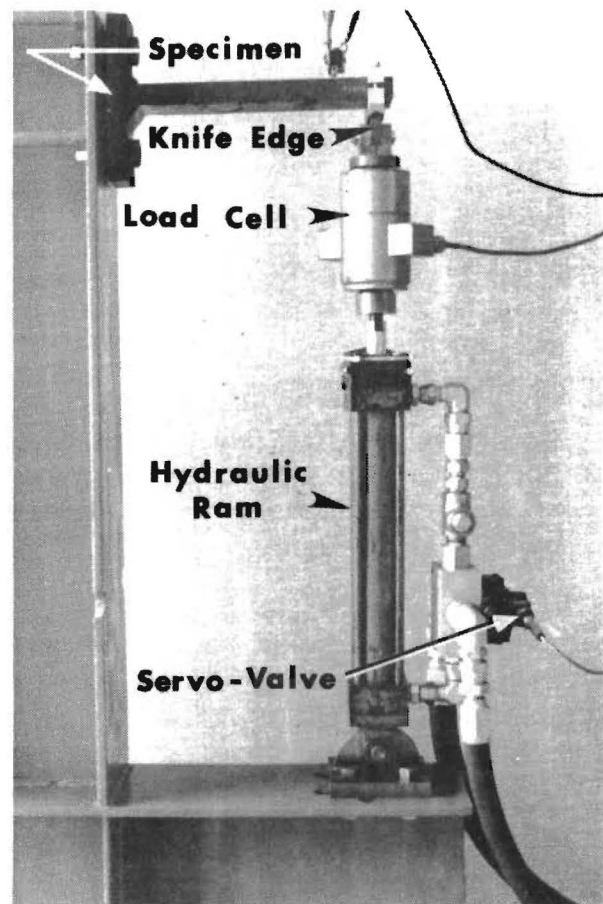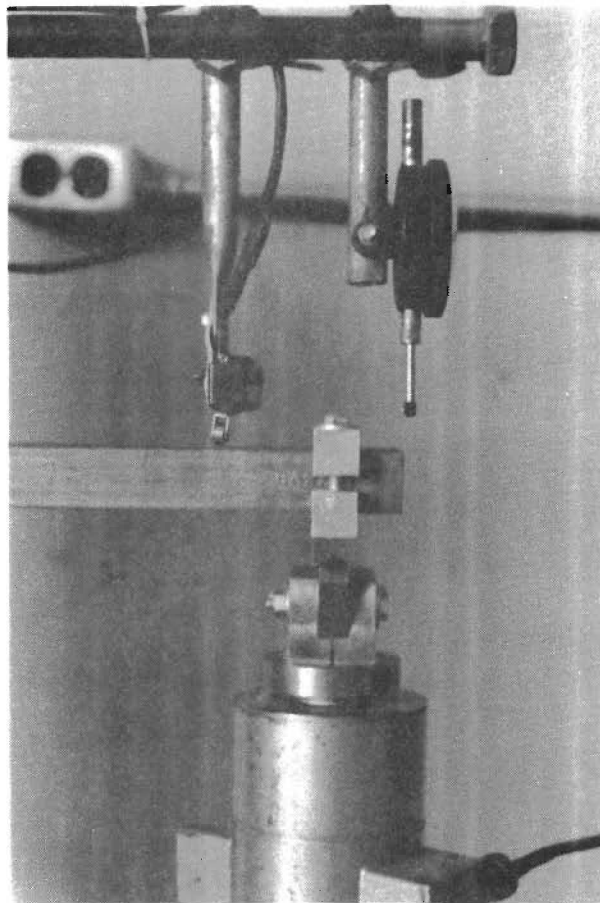he average of the two measurements made from each side of the knife edge support centerline to the weld toe on the tension side of the specimen. All tests were run with a minimum nominal tensile bending stress of 5 ksi at the weld toe.

The test was terminated when the error signal, which is the difference between the command signal and the feedback signal, increased by 10 percent of its initial value. This increase in error occurred due to stiffness changes within the cross-section where the fatigue crack grows.

The fatigue failure of the specimen starts from small surface cracks along the weld toe of the fusion line on the tensile loaded side of the specimen. The first visible cracking normally occurs near the center of the weld toe with other cracks initiating along the weld toe. These cracks grow as semi-elliptical cracks in planes offset slightly from one another due to the irregularities of the weld toe. The cracks eventually coalesce as shown in Fig. 2.6. The rings shown on the fracture surface in this figure were made by tinting the crack with dye penetrant after 62% of the total fatigue life. The two cracks shown coalesced together to form the large semi-elliptical crack. The resulting crack depths at the end of the tests were a quarter to half of the plate thickness as shown in Fig. 2.7. The fatigue crack depth is the elliptical smooth surface at the top of the plate in the figures.

In order to determine the magnitude of the additional life remaining in the uncracked section of the test specimen, one test was continued until the loading system was unable to maintain the desired loads. This occurred because the ram displacements had to increase to maintain the same level of loads as the section failed. The resulting
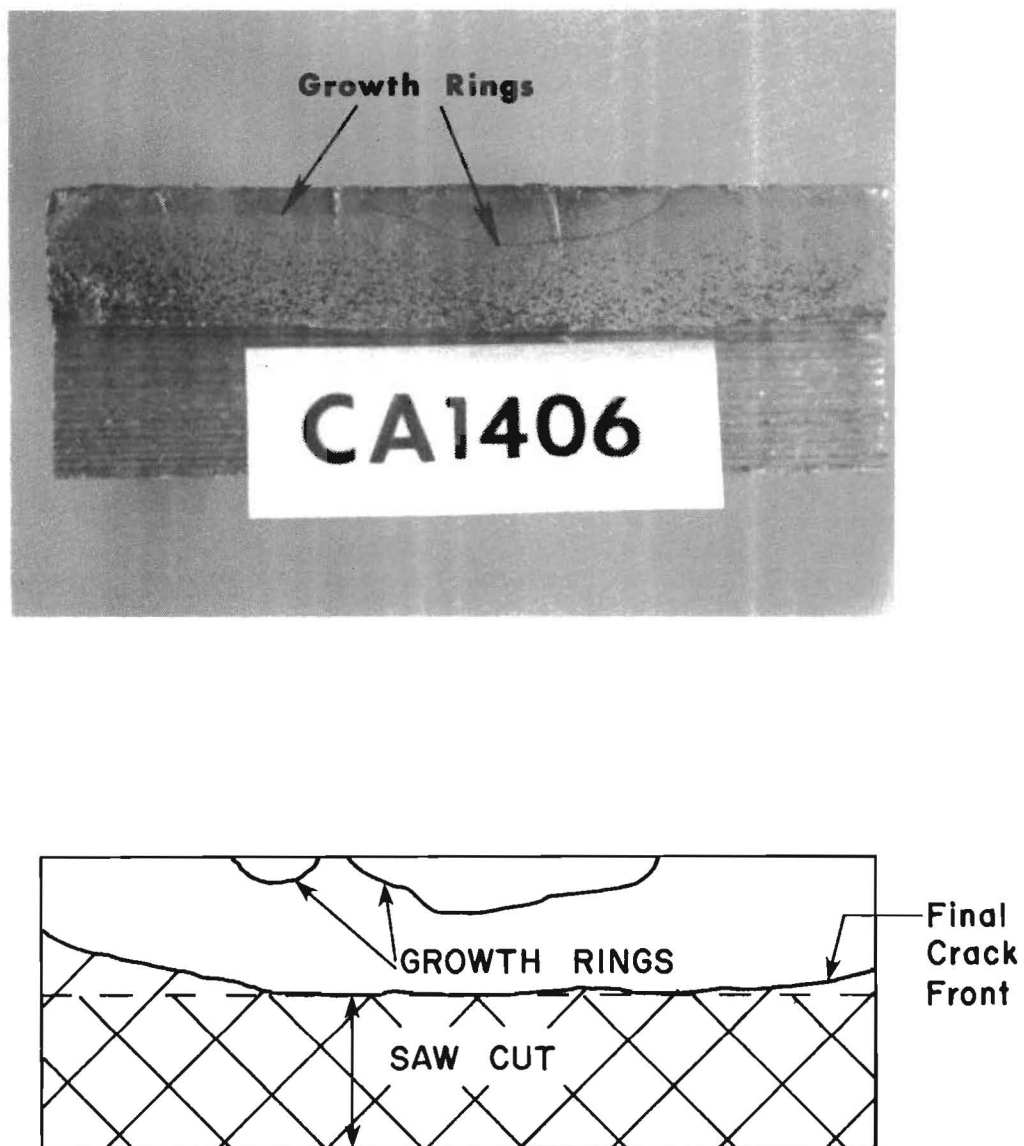
Fig. 2.6 Formation and growth of initial cracks in CA1406
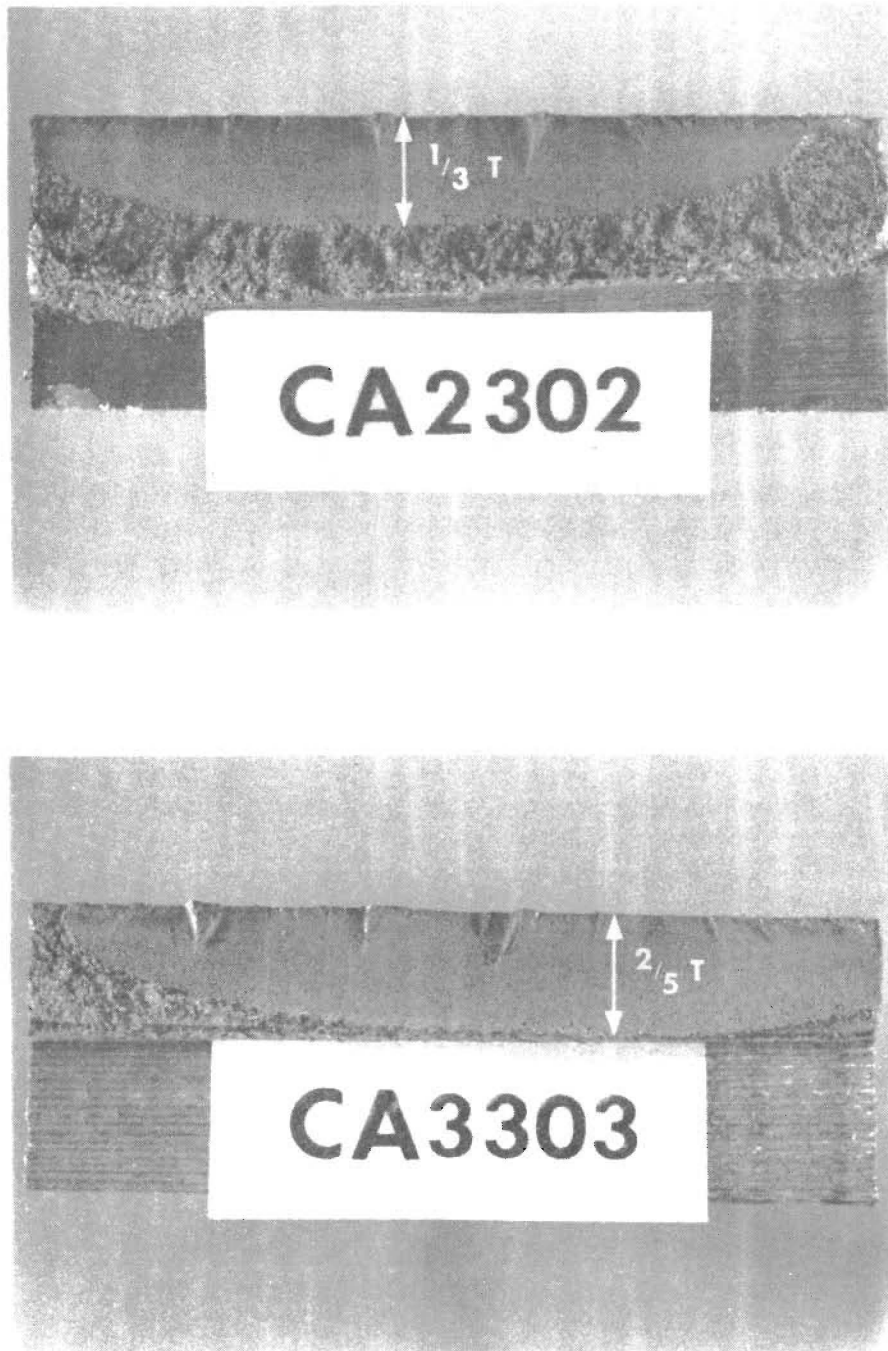
Fig. 2.7 Failure surfaces of two CA tests

crack shown in Fig. 2.8 is half the specimen thickness. The life consumed beyond the 10% error cutoff was 6%.

To further examine the rate of propagation, da/dN, dye penetrant was used to tint the crack of another specimen near the end of its test life as shown in Fig. 2.9. The amount of extension, Δa, is given by

$$\Delta a = a_f - a \simeq 0.45 \text{ in.} - 0.38 \text{ in.} = 0.07 \text{ in.}$$

The corresponding number of major cycles, ΔN, was 7280. The corresponding crack propagation ratio is $1/10^5$. Assuming that the rate of crack propagation does not increase, $\Delta N'$ (the number of cycles needed to grow the crack to midsection) is given by

$$\Delta N' \simeq (0.50 \text{ in.} - 0.45 \text{ in.}) \times 10^5 = 5000 \text{ cycles}$$

The test failure life was 393,810 cycles meaning that there was only a 1.3% potential increase in fatigue testing life. Remember, once the crack grew to mid-section, the experiment was halted as ram displacements became too large to attain the same load levels. It is concluded that there is no real difference in specimen test life when the crack is between one third to one half of the plate thickness.

2.5 SUPERIMPOSED SINE TESTING

In general, the stress distribution for an SS waveform based on reservoir counting can be expressed as shown in Fig. 2.10. The relative occurrence, γ, of major and minor stresses is a function of the number of minor stress excursions, z, present in an SS waveform.

Eight different waveforms were used for all the SS testing

Fig. 2.8 Crack grown to half of thickness
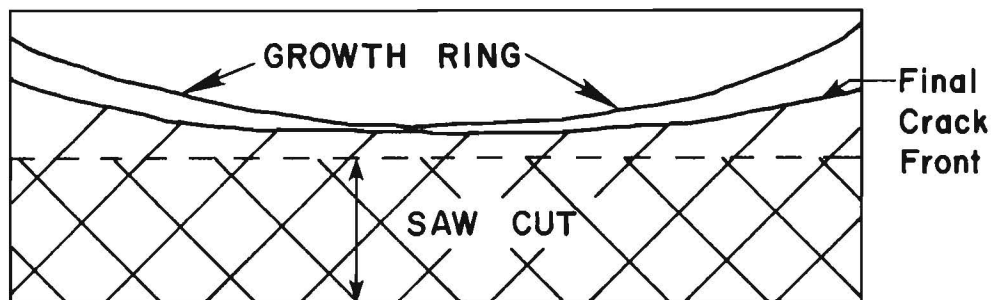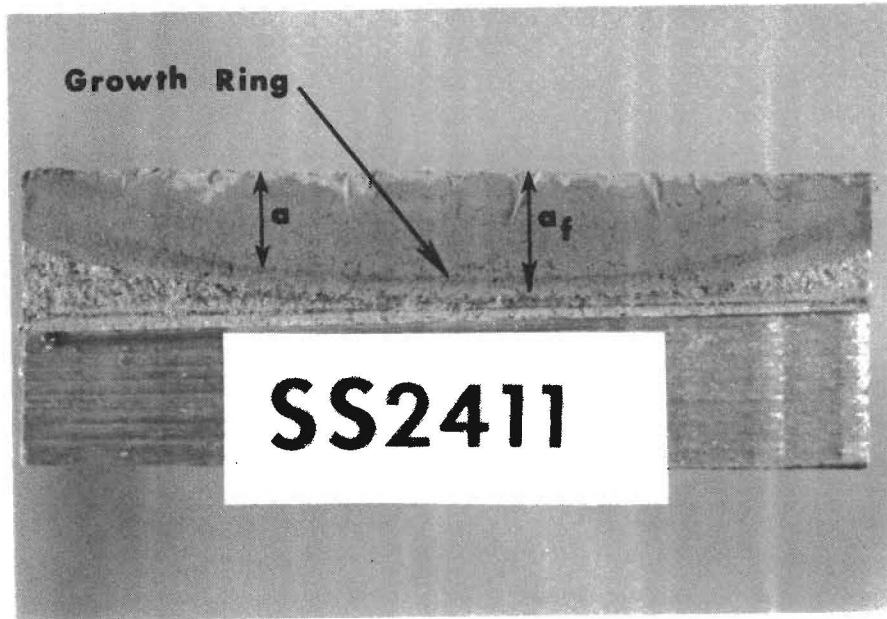
Fig. 2.9 Dye penetrant indication of crack extension
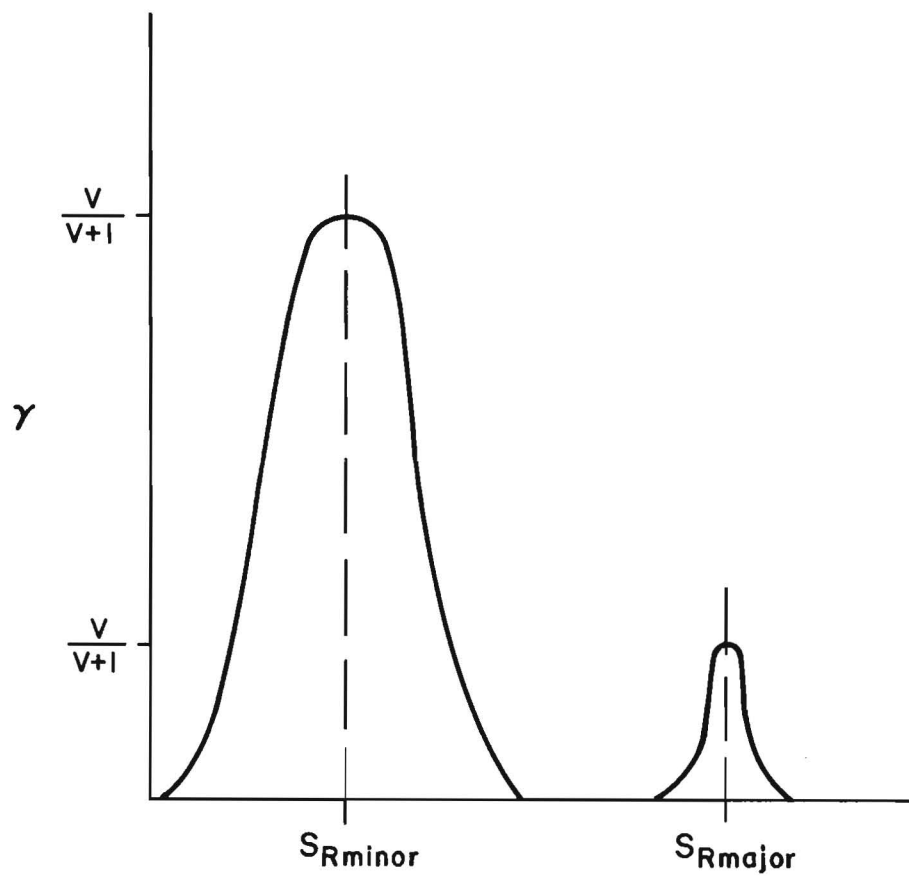
Fig. 2.10   Shape of SS stress distributions
(based on reservoir counting)
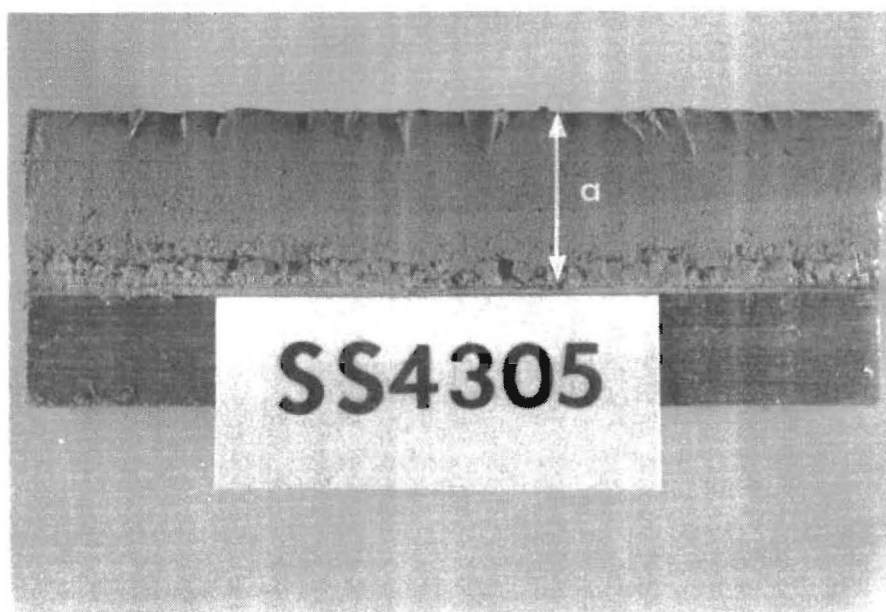
employed as shown in Table 2.2. This table shows the settings of the two function generator signals before summing. Table 2.2 also shows the effective stress range calculated for the major and minor stresses and will be called S_{Rmajor} and S_{Rminor} respectively. These effective stresses are evaluated using m = 4.2, since 4.2 is the slope of the CA data presented in Chapter 3. An effective major stress is determined using the major cycles of stress and similarly the effective minor stress is determined using all the minor stress excursions. These effective stresses were based on reservoir counted computer simulated stresses of the actual waveform. These values are then rounded to the values of σ and z shown in Table 2.2. These values of σ and z are used in discussing the effective major and minor stress respectively in the remainder of the text and will be used in all succeeding tables. The results of SS testing will be presented in two ways: 1) the effective stress range, S_{re} based on reservoir stress counting at the total number of cycles involved, N_t, and 2) the major stress range, σ, at the number of major stress cycles, N.

2.6 TEST LOAD MONITORING AND ACCURACY

In the constant amplitude, CA, tests, the peak to peak load values were monitored using a peak detector. The peak detector was used to initially set and maintain the desired absolute minimum and maximum load on the specimen. To ensure that the load signal shown on the peak detector corresponded to the load monitored by the electronic console, a shunt calibration test of the feedback signal was performed before every

TABLE 2.2 SUPERIMPOSED SINE, SS, TEST TYPES

| SS Test Type | Function Generator Settings | | | | (v+1) | Superimposed Sine Signal | | | |
| | Function Gen. #1 | | Function Gen. #2 | | | | | Nominal | |
	Frequency (Hz)	Amplitude	Frequency (Hz)	Amplitude		$^1S_{Rmajor}$ (ksi)	$^1S_{Rminor}$ (ksi)	σ (ksi)	z (ksi)
1	1	12.77	8	21.05	8	33.63	19.32	35	20
2	1/2	17.94	8	15.55	16	33.47	14.38	35	15
3	1	25.76	10	7.73	10	33.42	5.17	35	5.4
4	1	8.61	10	20.10	10	28.50	19.21	30	20
5	1	13.16	10	15.55	10	28.50	14.17	30	15
6	1	17.23	10	11.48	10	28.50	9.72	30	10
7	2	7.66	10	16.27	5	23.60	14.51	25	15
8	1	9.57	10	14.36	10	23.82	13.36	25	14

[1] m = 4.2

test run.

In the superimposed sine, SS, wave tests, only the absolute minimum and maximum peaks of the major wave were monitored. The SS testing presented certain problems as the SS waveform was created by summing two different function generator sine wave signals. It was impossible to eliminate the drift which existed between the function generator signals. This drift was caused by the drift in the frequencies and in the phasing of the signals at the start of the test. As a result, a variation in the major amplitude value occurred. Also, as sine waves are not linear functions, the superposition of the generated sine waves leads to a scatter of the minor wave amplitudes. These minor wave peaks could not be detected by the peak detector.

In order to estimate the resulting distribution of loads, computer simulation of the generated superimposed sine waves were performed for each type of superimposed sine waves used in the testing program to acquire a realistic distribution of stresses. Simulations of the actual SS waveforms were performed using the amplitudes and frequencies of the two function generator signals and selecting a frequency error between the two signals as demonstrated in the development of the following SS waveform using two sine waves.

The SS waveform with a major amplitude of $\sigma = 30$ ksi and nine excursions, $v = 9$, of minor amplitude of $z = 15$ ksi as shown in Fig. 2.11 will be approximated by the superposition of two sine waves. In order to have nine minor amplitudes, the frequency ratio, $v + 1$, between the two function generator signals must be ten. Since a small frequency error occurs between the signals, let one signal run at 1 Hz and the other signal at 10.05 Hz. This will cause one minor wave to drift in every 20 cycles of the major waveform. If the respective programmed amplitudes are 13.92 and 16.25, then one cycle of the resulting complex

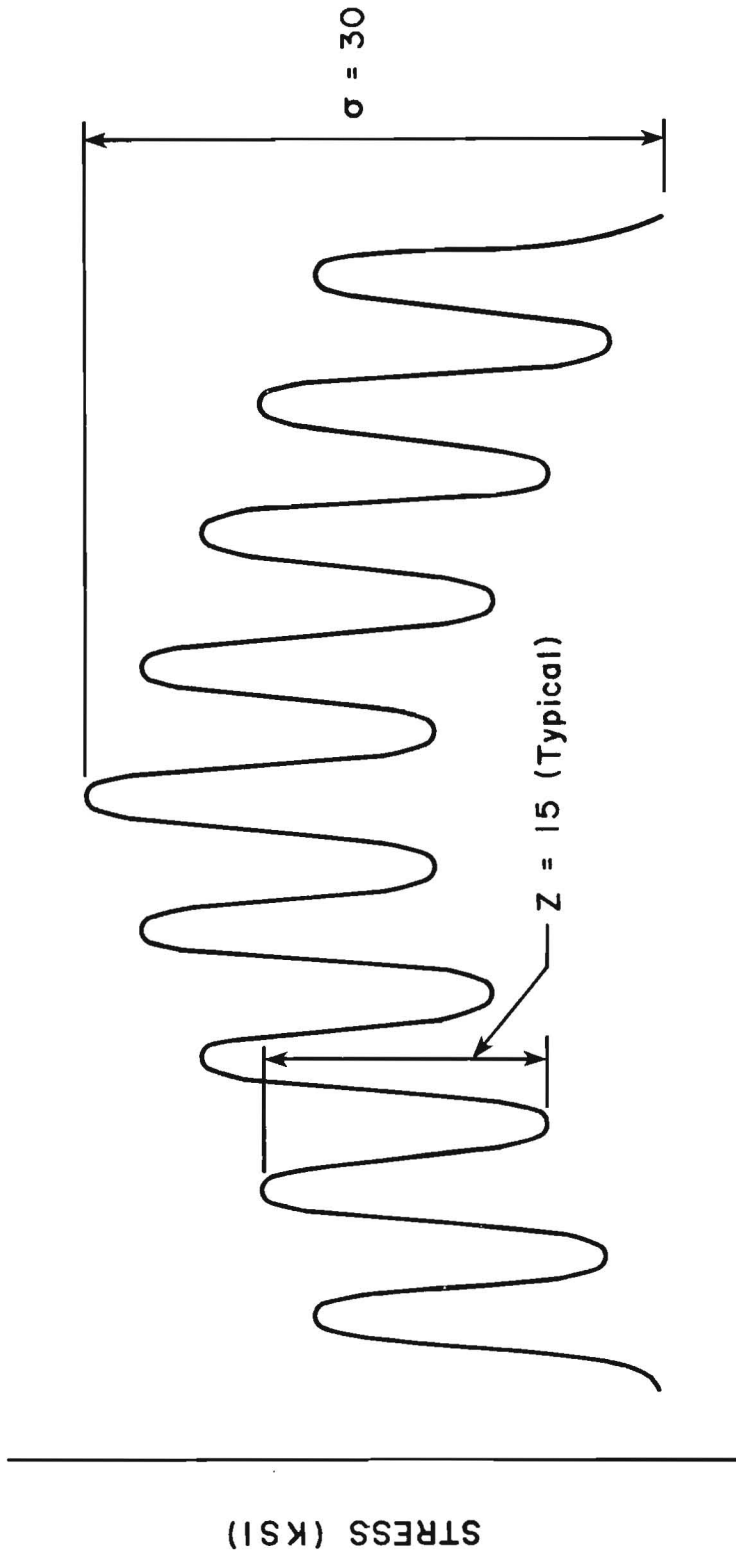σ = 30

Z = 15 (Typical)

STRESS (KSI)

Fig. 2.11 Desired waveform

waveform is shown in Fig. 2.12. The scatter of stress ranges associated with the minor amplitude is 14.1 to 15.7 ksi and the major amplitude is 29.9 to 30.2 ksi. The corresponding stress histogram is shown in Fig. 2.13. A high speed digital data acquisition system was employed to verify some of the simulation tests. High speed recordings were made from the load cell output of actual test loads on the specimen using a fixed sampling speed of 84 samples per second. The ability of the high speed recorder to sample the absolute minimum and maximum values diminishes at higher input frequencies due to the fixed sampling rate. The rolloff of the recording system was determined using a constant amplitude sine signal run at the same frequency as the high frequency minor wave signal portion of the SS waveform. Figure 2.14 shows a histogram of the recorded load range divided by the programmed load range for 36 cycles of loading at 10 Hz. The largest recorded load range is 96% of the actual with a mean of 95.4% for the recorded data. A similar analysis of a 1 Hz input sine wave produced a mean measured load range of 99.6%. This implies that the digital recorder is accurate and that the inaccuracy is attributable to sampling. Thus, all digitally recorded SS waveforms with minor wave frequencies of 10 Hz were corrected by dividing recorded stress ranges by 0.954. Figure 2.15 shows a stress range histogram for a particular SS test where the stress range predicted by computer simulation and recorded data during experimental testing divided by 0.954 is presented. The results indicate that the computer simulated stresses exceed the recorded stresses by less than 0.5 ksi. This implies that the actual stresses are slightly lower than predicted, meaning that fatigue lives of the SS testing should be longer than predicted.

An effective major and minor stress is calculated in Table 2.3 for the stress histogram of Fig. 2.15. Also, an effective stress based
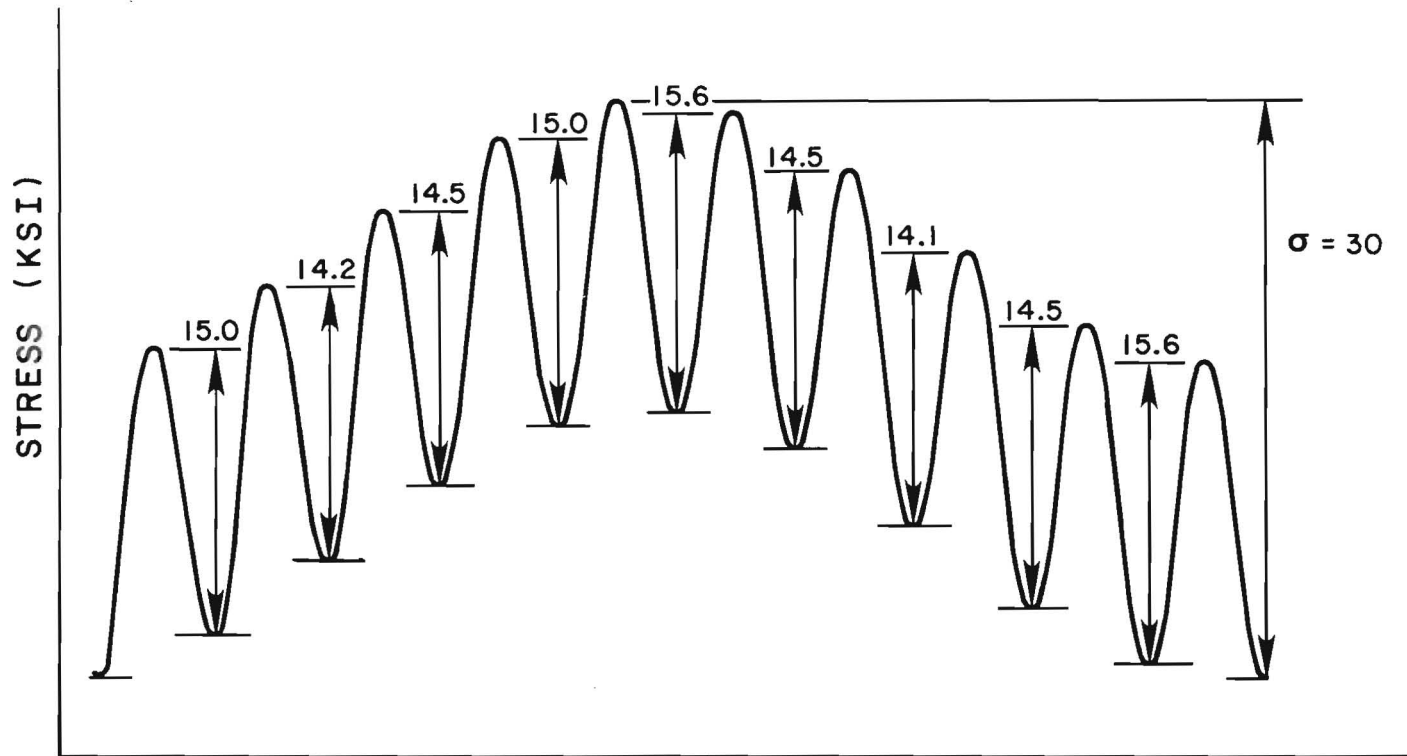
Fig. 2.12 Waveform from superposition of two sine waves
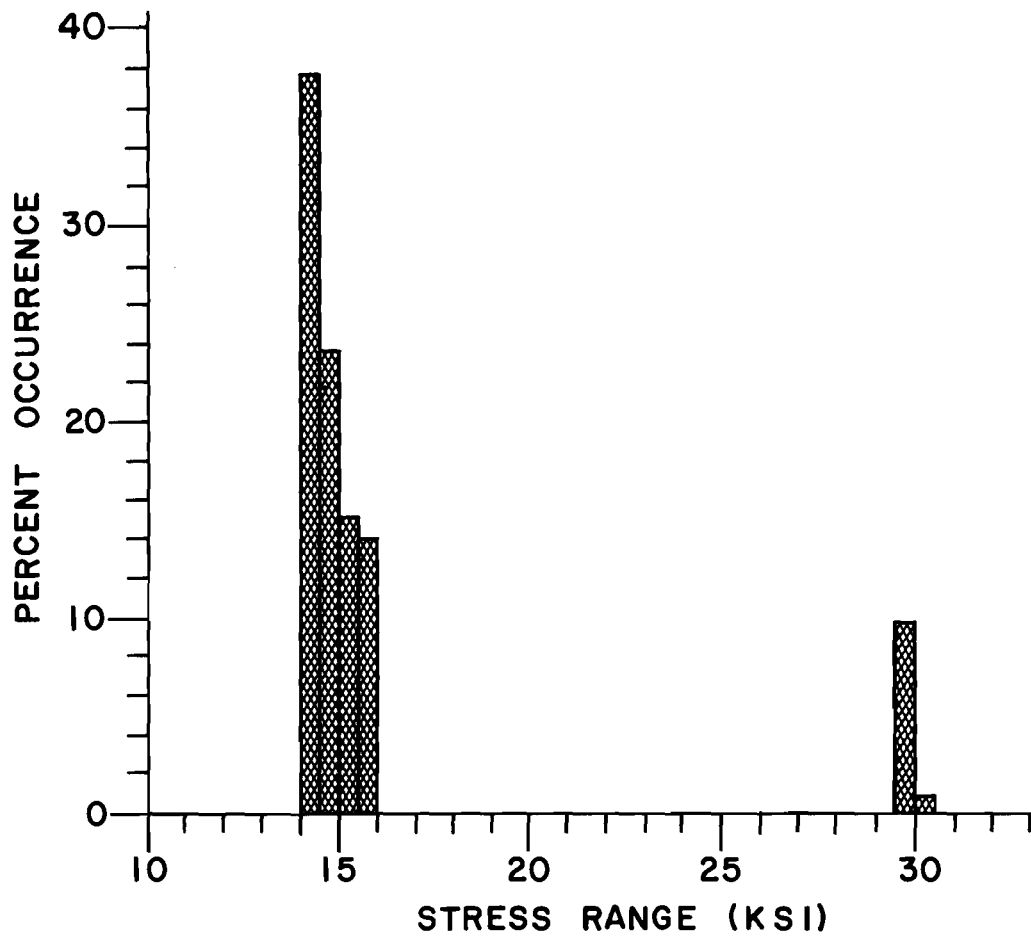
Fig. 2.13   Stress histogram of a computer simulated waveform
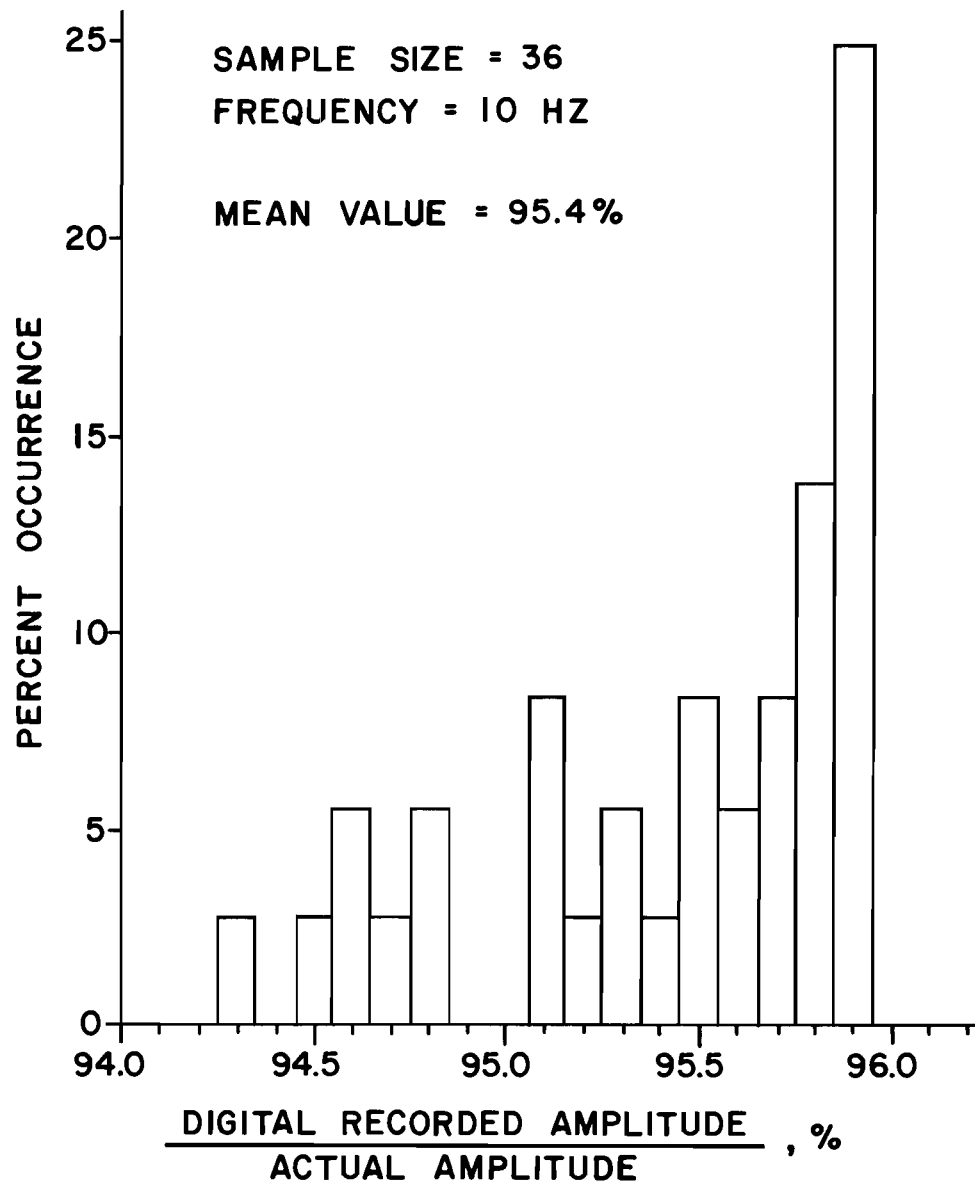
Fig. 2.14 Digital recorded amplitudes of a constant sine amplitude signal at 1 Hz
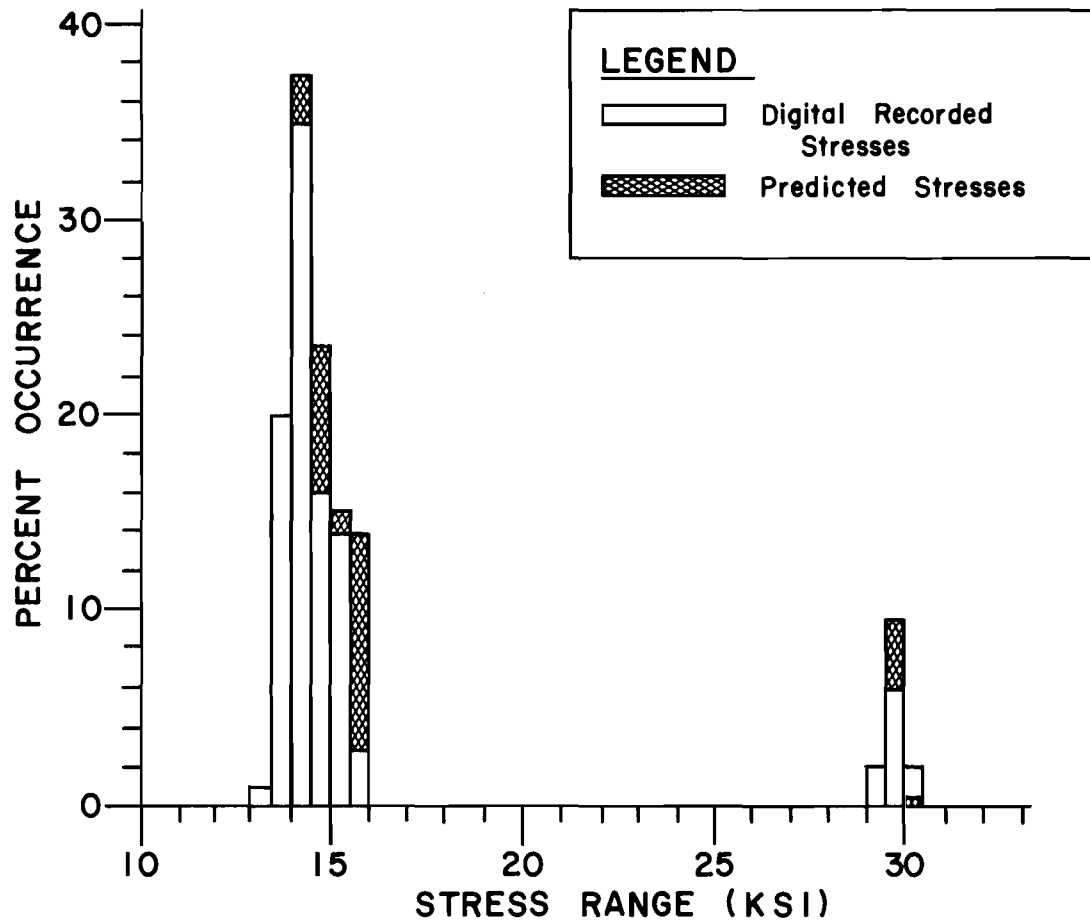
Fig. 2.15 Stress histogram of SS3306

TABLE 2.3 COMPARISON OF EFFECTIVE STRESS CALCULATIONS FOR STRESS
HISTOGRAM OF FIGURE 2.15

	[1]Effective Stress (ksi)		
	Major	Minor	Major & Minor
Computer Simulated	29.8	14.8	18.9
Hi-Speed Digital/0.954	29.3	14.4	18.8
Reported	30.0	15.0	19.1
Reported/Digital	1.02	1.04	1.02

[1]$m = 4.2$

on the overall stress histogram is provided using $m = 4.2$ in Table 2.3. These effective stresses, determined from computer simulation and high speed digital recording, are compared with each other. The effective major and minor stress predicted from computer simulation as shown in Table 2.3 are within 4% of the respective digital recorded effective major and minor stress. The corresponding effective stress of the entire computer simulated stress histogram is within 2% of the entire digital recorded stress histogram when $m = 4.2$. This implies good correlation between the stresses predicted and recorded. Thus, the stresses predicted from the computer simulation can be taken as the actual stresses and will be used to report the test results.

CHAPTER 3: TEST RESULTS

3.1 CONSTANT AMPLITUDE TEST RESULTS

Constant amplitude, CA, tests were conducted on 4 weldment groups to establish an S-N curve to serve as a basis to evaluate the complex stress function results. All of the CA test results are summarized in Table 3.1 and are plotted on a log-log S-N plot shown in Fig. 3.1. Note that weldment 1 test results produced the longest lives. The same results plotted in Fig. 3.1 are plotted in Fig. 3.2 along with a best fit regression line for each weldment type. In Fig. 3.2, the regression lines of weldments 2, 3, and 4 nearly lay on top of one another. The similarity of the regression lines of weldments 2, 3, and 4 indicate that they have the same behavior in constant amplitude fatigue. The CA results of weldment 1 did not correlate well those of weldments 2, 3, and 4. Thus, an S-N curve based only on weldments 2, 3, and 4 was established to evaluate the superimposed sine, SS, test results. SS testing was restricted to only weldments 2, 3, and 4 so that results could readily be compared between weldment groups. Note that weldments 2, 3, and 4 will be treated as producing identical behavior when comparing SS to CA test results. A plot of this standard CA data considering only weldments 2, 3, and 4 is shown in Fig. 3.3. The slope of the mean regression line is 4.2. Included in the plot, is a two sided 95% confidence band of the mean line. All CA testing performed on weldments 2, 3, and 4 resulted in specimen failure. The lowest CA test level run was 12.5 ksi for a weldment 4 specimen which failed at 22.3 million cycles.

TABLE 3.1   CONSTANT AMPLITUDE, CA, TEST RESULTS

Test Specimen	Weldment Number	Stress Range (ksi)	Cycles to Failure $x10^3$
CA1201	1	33.42	566
CA1205	1	33.46	411
CA2203	2	33.46	210
CA2204	2	33.46	338
CA1302	1	28.71	645
CA2302	2	28.68	584
CA3301	3	28.65	693
CA3303	3	28.71	422
CA4301	4	28.65	541
CA1403	1	23.90	1,182
CA1406	1	23.92	1,870
CA2401	2	23.82	1,064
CA2405	2	23.93	1,433
CA3402	3	23.87	1,105
CA4403	4	23.90	1,138
CA4404	4	23.92	1,062
CA1504	1	19.16	[1]9,739
CA2506	2	19.12	2,095
CA4502	4	19.12	3,873
CA3610	3	17.19	4,245
CA4710	4	14,35	9,314
CA4812	4	11.98	22,460

[1] Test discontinued
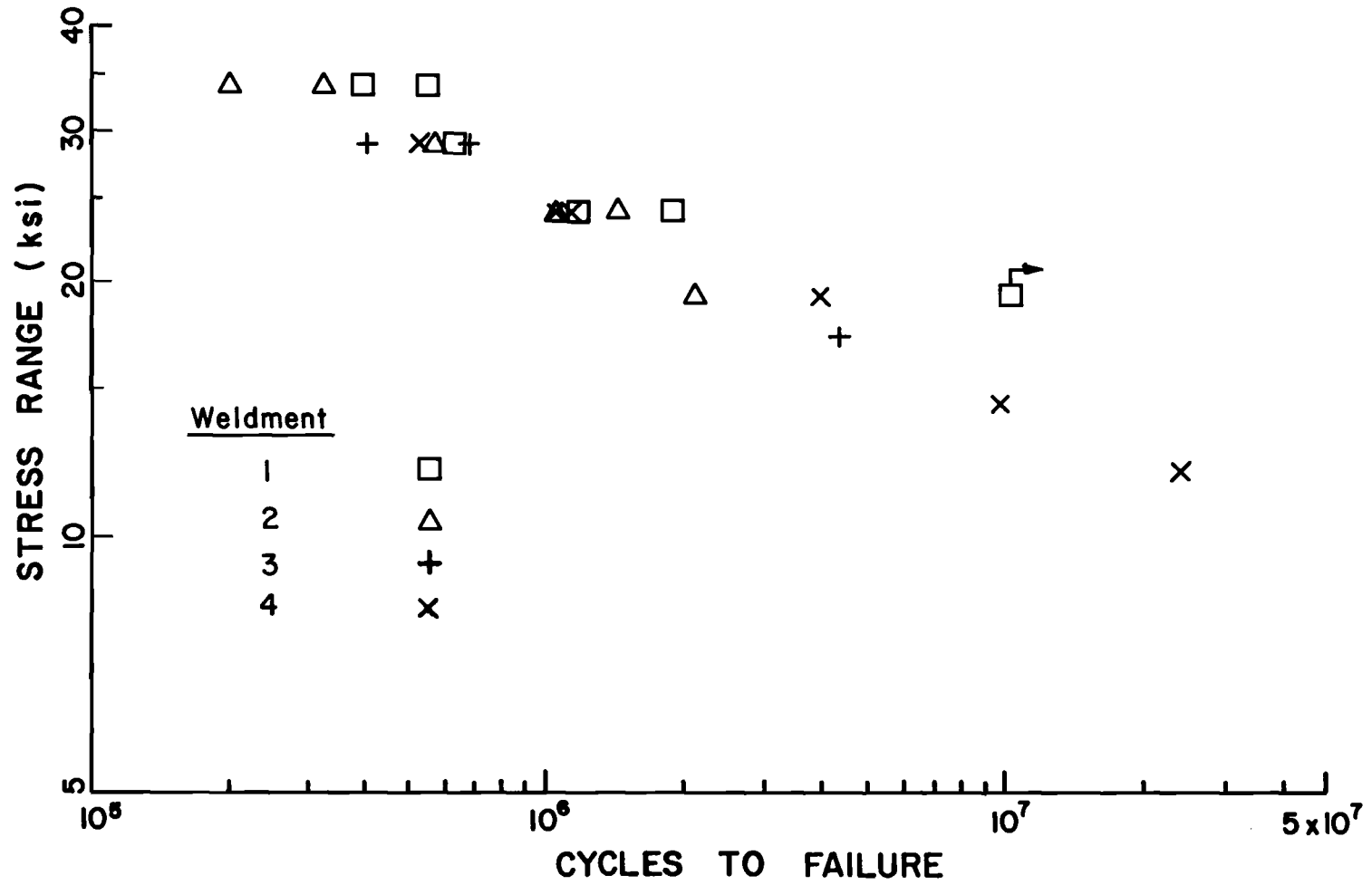
Fig. 3.1 Constant amplitude test data
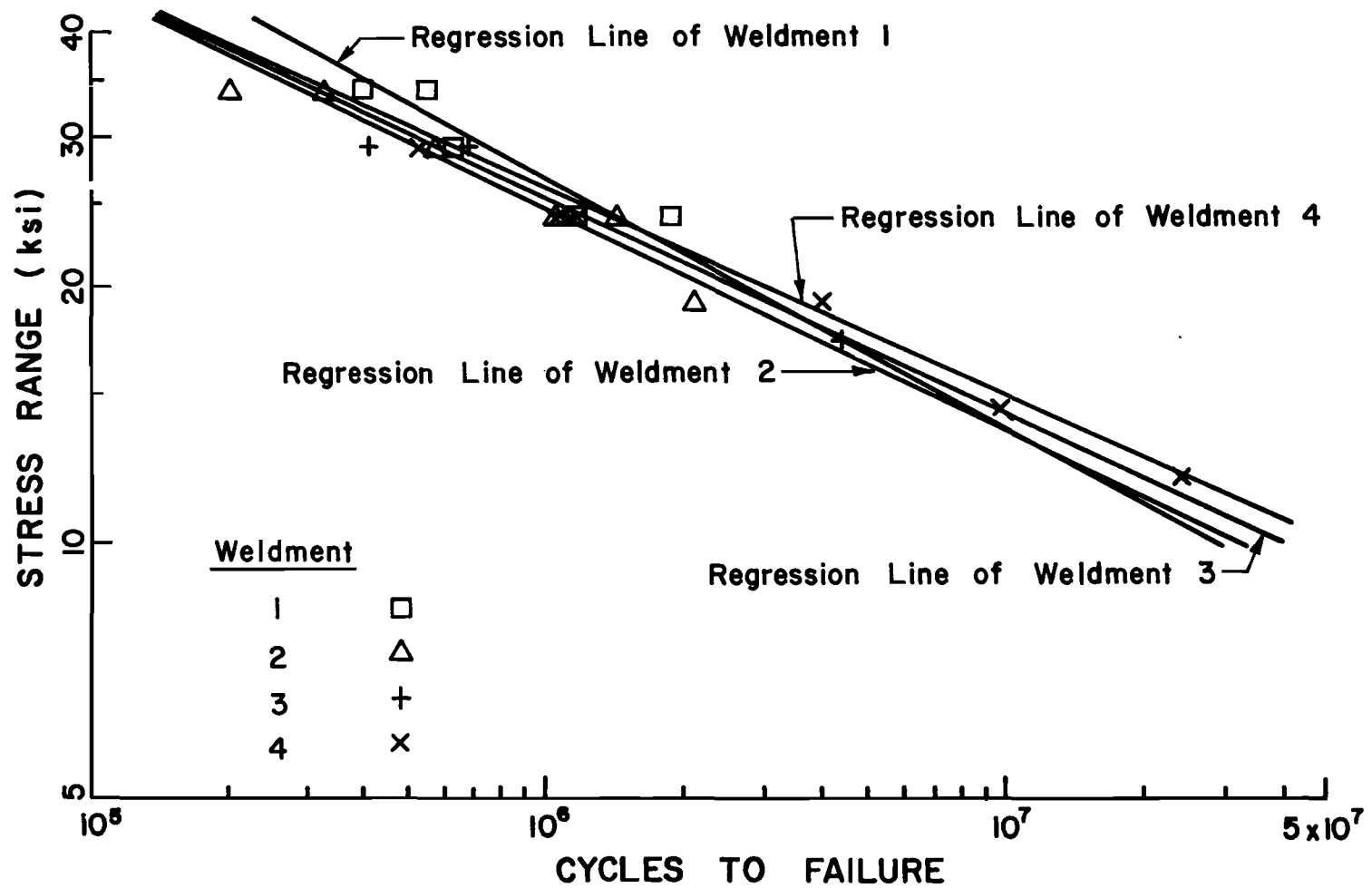
Fig. 3.2 Constant amplitude test data with best fit of each weldment group

The chart shows STRESS RANGE (ksi) on the vertical axis versus CYCLES TO FAILURE on the horizontal axis, with the following annotations:

95 % Confidence limit of regression line

$$N = 7.03 \times 10^{11} \, S_R^{-4.19}$$

Weldment

2	△
3	+
4	×
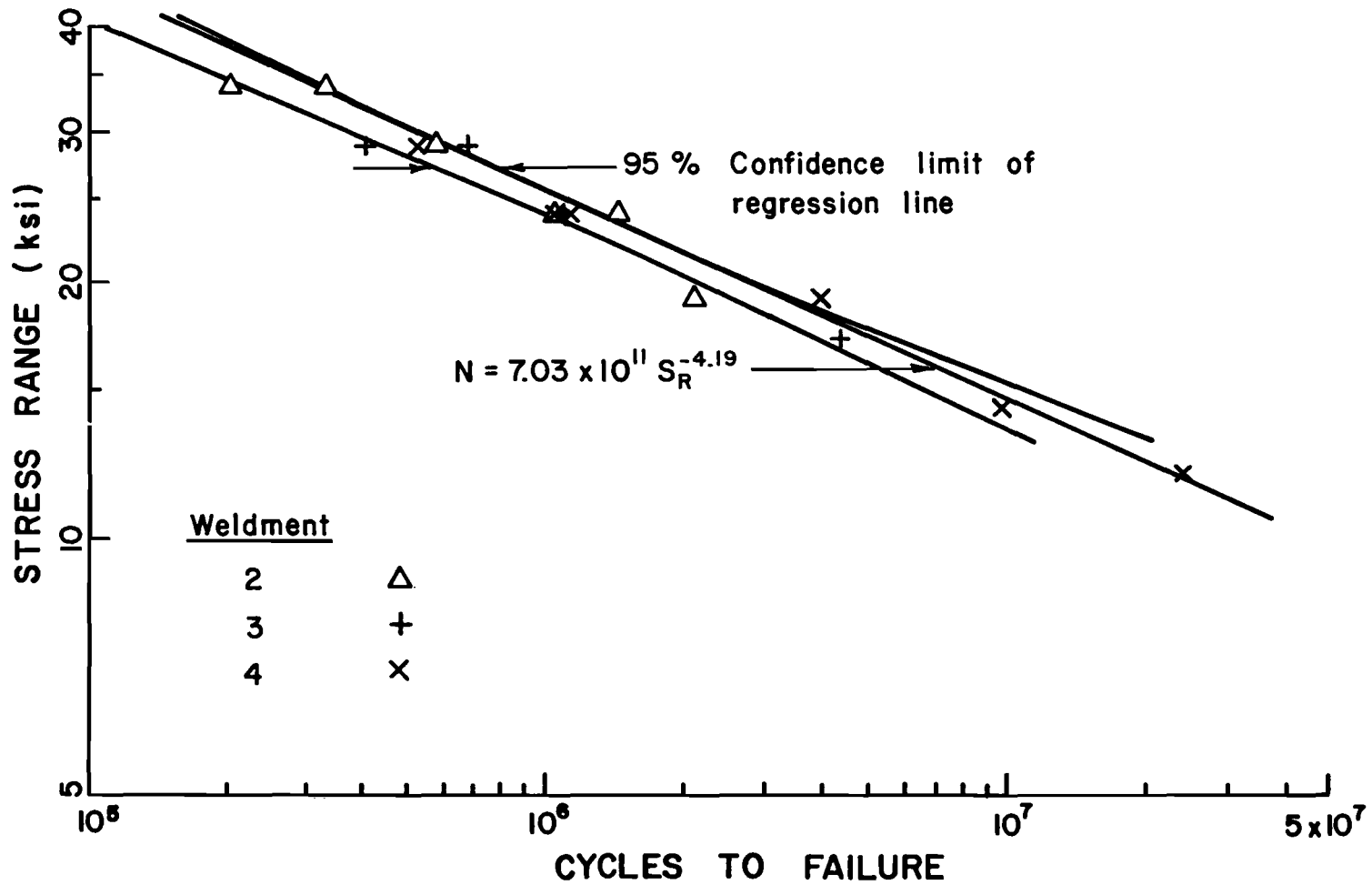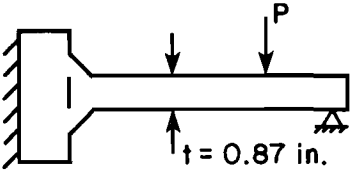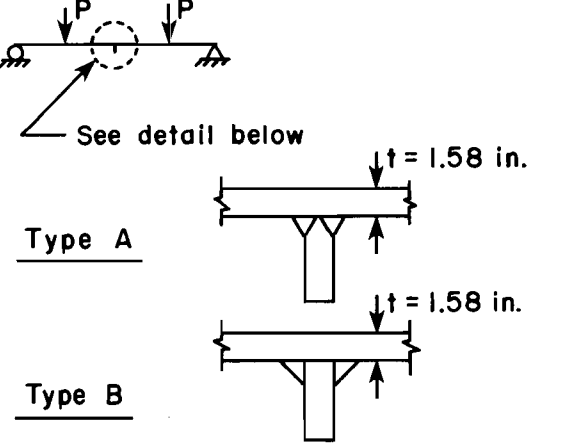
Fig. 3.3 Standard S-N curve based on weldments 2, 3, and 4

Other investigators [1,6,8,13] have conducted fatigue tests on various as-welded bending specimens. The type of loading and specimen geometry varied in these investigations. Table 3.2 shows schematically the types of specimens and weld geometry used in these studies. The results of previous studies along with all of the CA results of this present study are plotted in Fig. 3.4. In general, the lives of the CA tests conducted in this study had longer fatigue lives. All the slopes of the S-N curves were comparable with the exception of those in ref. 1 which had a flatter slope (a larger value of the stress range exponent). Tests from refs. 1 and 13 produced shorter lives. This could be due to the fact that the plate thicknesses were larger in these tests than in the other tests reported, which would correlate with Gurney's findings that thicker specimens should produce shorter lives [3]. Also, a 4 point bending load scheme was employed in refs. 1 and 13 as opposed t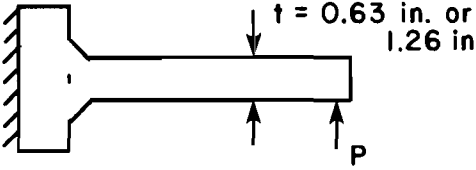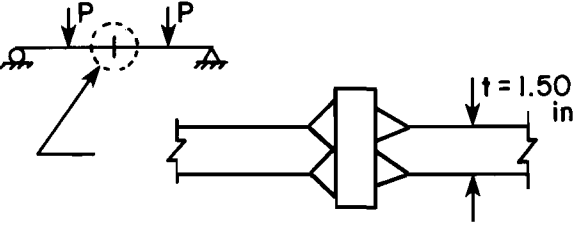o cantilever bending used in the other studies. Only one set of data [1] plotted used fully reversed loading (R = -1). Since no significant difference in the test results occurred when the stress ratio, R, was equal to 0 or -1, no distinction of R was made in plotting this data. Overall, the test results of this study appear to show fatigue behavior that is consistent with other investigations.

TABLE 3.2 BENDING SPECIMENS USED IN OTHER INVESTIGATIONS

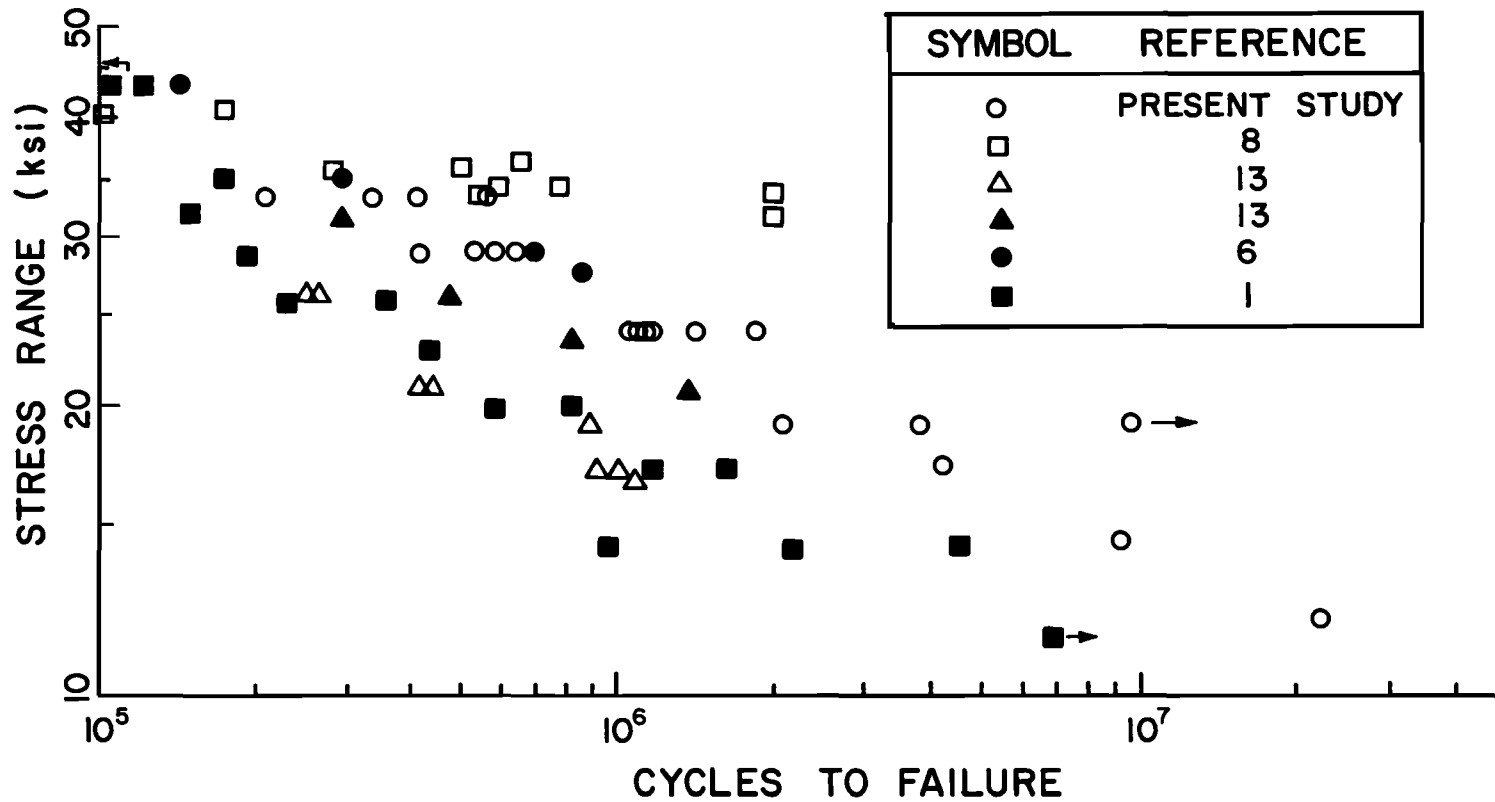| Specimen Type and Loading	Weld	R	Ref.
t = 0.63 in. or 1.26 in.	Partial Penetration Fillet	0.1	8
t = 1.50 in.	Full-Penetration Fillet	0 and -1	1
t = 0.87 in.	Fillet	0.1	6
See detail below Type A t = 1.58 in. Type B t = 1.58 in.	Non-Load Carrying Weld Type A: Full-Penetration Fillet Weld Type B: Fillet Weld	0.1	13

Fig. 3.4 Constant amplitude test data on bending specimens

3.2 SUPERIMPOSED SINE TEST RESULTS

All superimposed sine, SS, test results are summarized in Table 3.3. In order to determine the significance of the minor stress ranges, z, upon the fatigue life of the specimens, the major stress range, σ, was plotted with the corresponding number of major cycles to failure, N, in Fig. 3.5. All of the data except one test result falls to the left of the 95% confidence limit for the corresponding CA regression line indicating that the smaller stress cycles produce a significant reduction in the fatigue life. A similar result occurs when the effective stress range, S_{re}, was plotted with the total number of cycles to failure, N_t, as shown in Fig. 3.6. S_{re} is determined using m = 4.2 in this figure. This plot has a better correlation with the CA line than did the plot of σ vs. N. However most of the fatigue results in this plot fell short of the predicted fatigue life. Therefore, the linear cumulative damage model used to calculate S_{re} does not appear to adequately account for all damage occurring from the small stress cycles.

Initially one purpose of the study was to investigate whether minor wave damage could be represented in variable amplitude testing by cumulative damage rules where stresses are determined from reservoir counting techniques. Two sets of experiments were initiated as discussed in Section 1.8 on weldments 3 & 4 respectively.

In weldment 3, 3 pairs of SS tests were conducted. The minor stress range, z, was kept constant at 15 ksi, while the major stress range, σ, and the stress sequences, v + 1, were varied so that S_{re} was constant at approximately 18 ksi when using a root mean cubed effective stress, S_{rmc}, calculation. This implies that the lives of the test specimens should be the same. It is apparent when viewing Table 3.4 that

TABLE 3.3   SUPERIMPOSED SINE, SS, TEST RESULTS

Test Specimen	Weld-ment No.	$(v+1)$	Nominal σ (ksi)	Nominal z (ksi)	$\dfrac{z}{\sigma}$	$^1S_{rr}$ (ksi)	N x10^3	N_t x10^3
SS2207	2	10	35	5.4	0.154	19.3	183.0	1,830
SS2208	2	10	35	5.4	0.154	19.3	339.2	3,392
SS3204	3	16	35	15	0.429	18.9	85.2	1,363
SS3205	3	16	35	15	0.429	18.9	91.1	1.457
SS2209	2	8	35	20	0.571	23.2	140.9	1,127
SS2210	2	8	35	20	0.571	23.2	163.8	1,311
SS4306	4	10	30	10	0.333	16.8	224.7	2,247
SS4309	4	10	30	10	0.333	16.8	203.8	2,038
SS3306	3	10	30	15	0.500	18.1	187.3	1,873
SS3307	3	10	30	15	0.500	18.1	195.3	1,953
SS4305	4	10	30	15	0.500	18.1	181.4	1,814
SS4311	4	10	30	20	0.500	18.1	198.6	1,986
SS4307	4	10	30	20	0.667	20.9	133.4	1,334
SS4308	4	10	30	20	0.667	20.9	164.4	1,644
SS2411	2	10	25	14	0.560	15.8	393.8	3,938
SS2412	2	10	25	14	0.560	15.8	503.7	5,037
SS3408	3	5	25	15	0.600	17.8	392.6	1,963
SS3409	3	5	25	15	0.600	17.8	435.6	2,178

^{1} $m = 4.2$
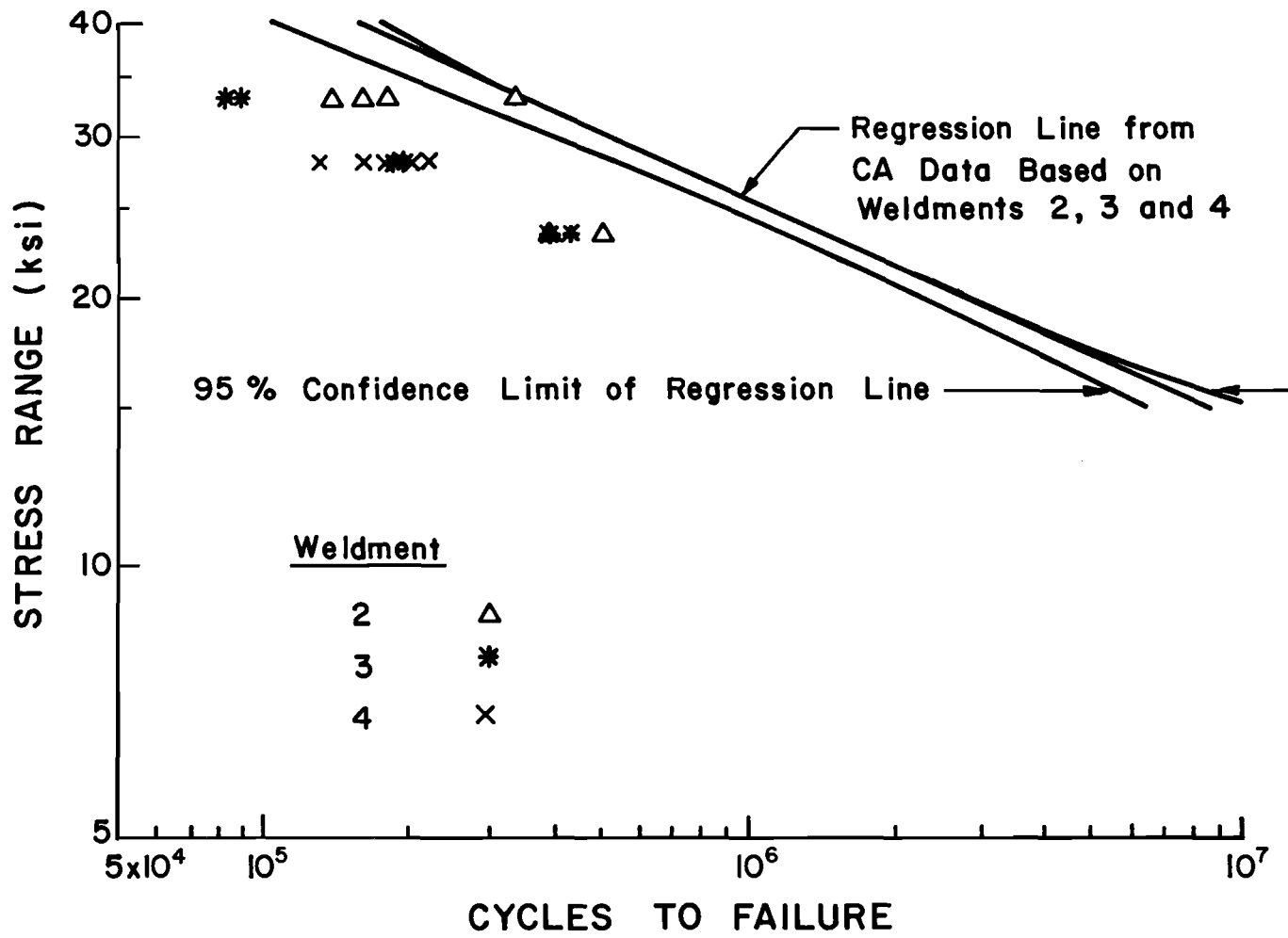
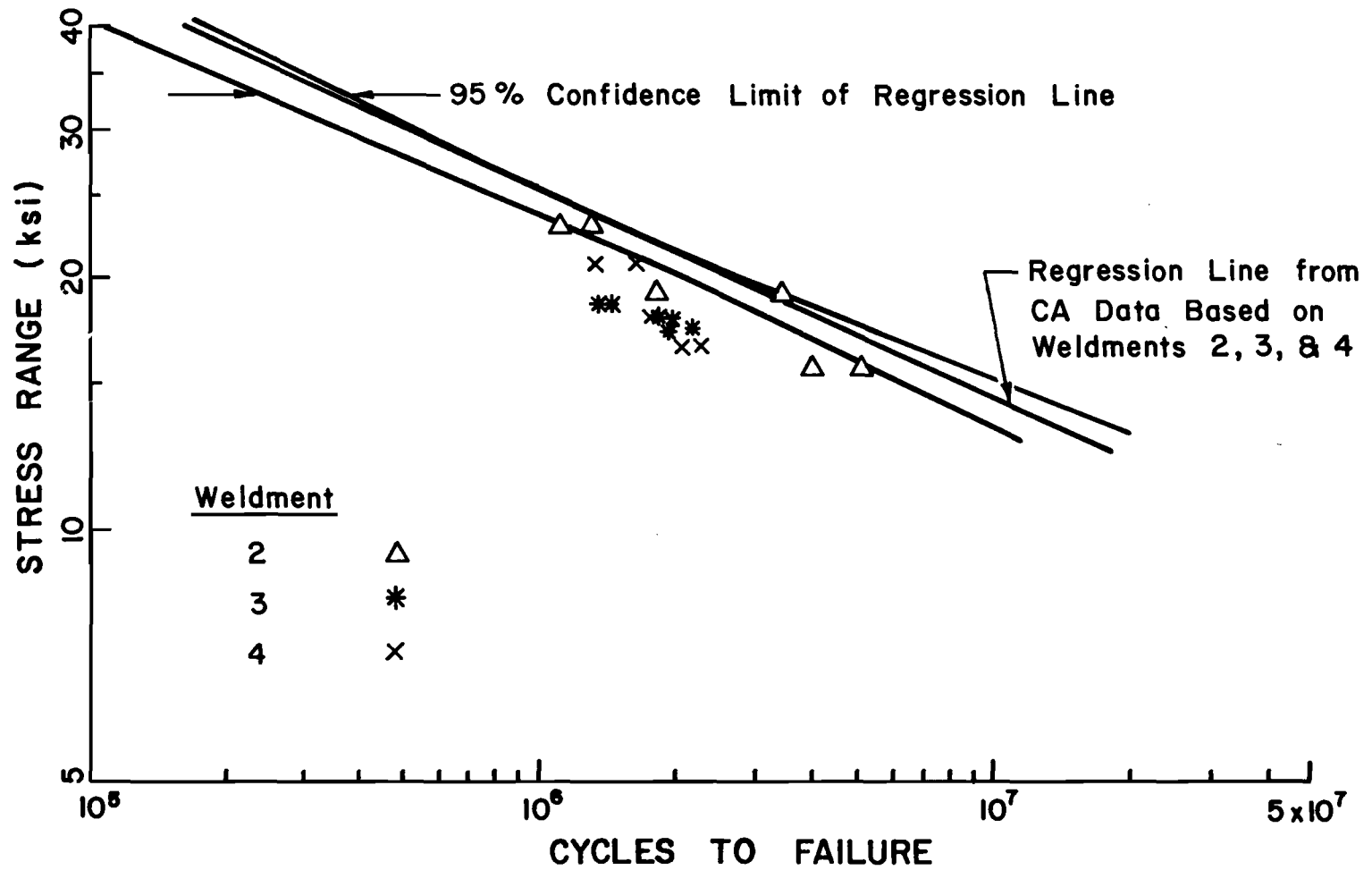Fig. 3.5   Plot of σ vs. N for superimposed sine testing

Fig. 3.6 Effective stress of superimposed sine tests (m = 4.2) vs. fatigue life

TABLE 3.4   WELDMENT 3:   SS TEST SUMMARY

[1]Spcmn	Nominal σ (ksi)	v+1	Nominal p	N_t x10^3	[2]N_{pred}	[2]%N_t	[3]N_{pred}	[3]%N_t
SS3204	35	16	.429	1,363	4,667	.292	3,226	.423
SS3205	35	16	.429	1,457	4,667	.312	3,226	.452
SS3306	30	10	.500	1,873	5,013	.374	3,831	.489
SS3307	30	10	.500	1,953	5,013	.390	3,831	.510
SS3408	25	5	.600	1,963	4,743	.414	4,113	.477
SS3409	25	5	.600	2,178	4,743	.459	4,113	.530

[1] z = 15 ksi

[2] N_{pred} is based on S_{rr} using m = 3 and is x 10^3

[3] N_{pred} is based on S_{rr} using m = 4.2 and is x 10^3

TABLE 3.5   WELDMENT 4:   SS TEST SUMMARY

[1]Specimen	Nominal z (ksi)	Nominal p	N_t x10^3	[2]N_{pred}	%N_t
SS4306	10	.333	2,247	5,164	.435
SS4309	10	.333	2,038	5,164	.395
SS4305	15	.500	1,814	3,831	.474
SS4311	15	.500	1,986	3,831	.518
SS4307	20	.667	1,334	2,084	.640
SS4308	20	.667	1,644	2,084	.789

[1] σ = 30 ksi and v+1 = 10

[2] Based on S_{rr} using m = 4.2

the life corresponding to S_{rmc} shows no relation to the actual fatigue lives. Although an S_{re} based on m = 4.2 gave better fatigue life predictions, the predicted lives were much larger then the experimental results. Also, as the major stress range decreased, the fatigue life increased and the predicted lives were closer to the actual.

In weldment 4, 3 pairs of SS tests were performed to determine the damage effect of minor stress, z. The minor stress, z, was varied, while the major stress, σ, and the ratio "v + 1" were held constant at 30 ksi and 10 respectively. Table 3.5 summarizes the results. The results of Table 3.5 show that for smaller values of z, the ratio of the actual failure life to the predicted failure life decreased. This implies that there is a non-linear damage interaction between minor stress, z, and major stress, σ. This is similar to the effect found in the results from weldment 3.

A plot of p, z/σ, against the ratio of the predicted average fatigue life, N_{avg}, using S_{re} divided by the actual number of total cycles to failure, N_t, is shown in Fig. 3.7 for all the SS tests. The bars shown in the figure represent the range of the individual test results. The scatter in the figure is large, however it does indicate that the error in the fatigue life estimation is not constant with "z/σ". The maximum error occurs in the vicinity of p equal to 0.3 to 0.4. The corresponding fatigue life is overestimated by a factor of two or more. When discussing Gurney's model in section 1.6, where S_{rg}/S_{rr} was plotted against z/σ, the maximum value of S_{rg}/S_{rr}, the ratio of Gurney's effective stress to the linear cumulative damage model stress, for values of "v" between 5 and 15 occurred in the same range of "p". This would indicate that Gurney's effective stress should provide a better estimate of fatigue performance.

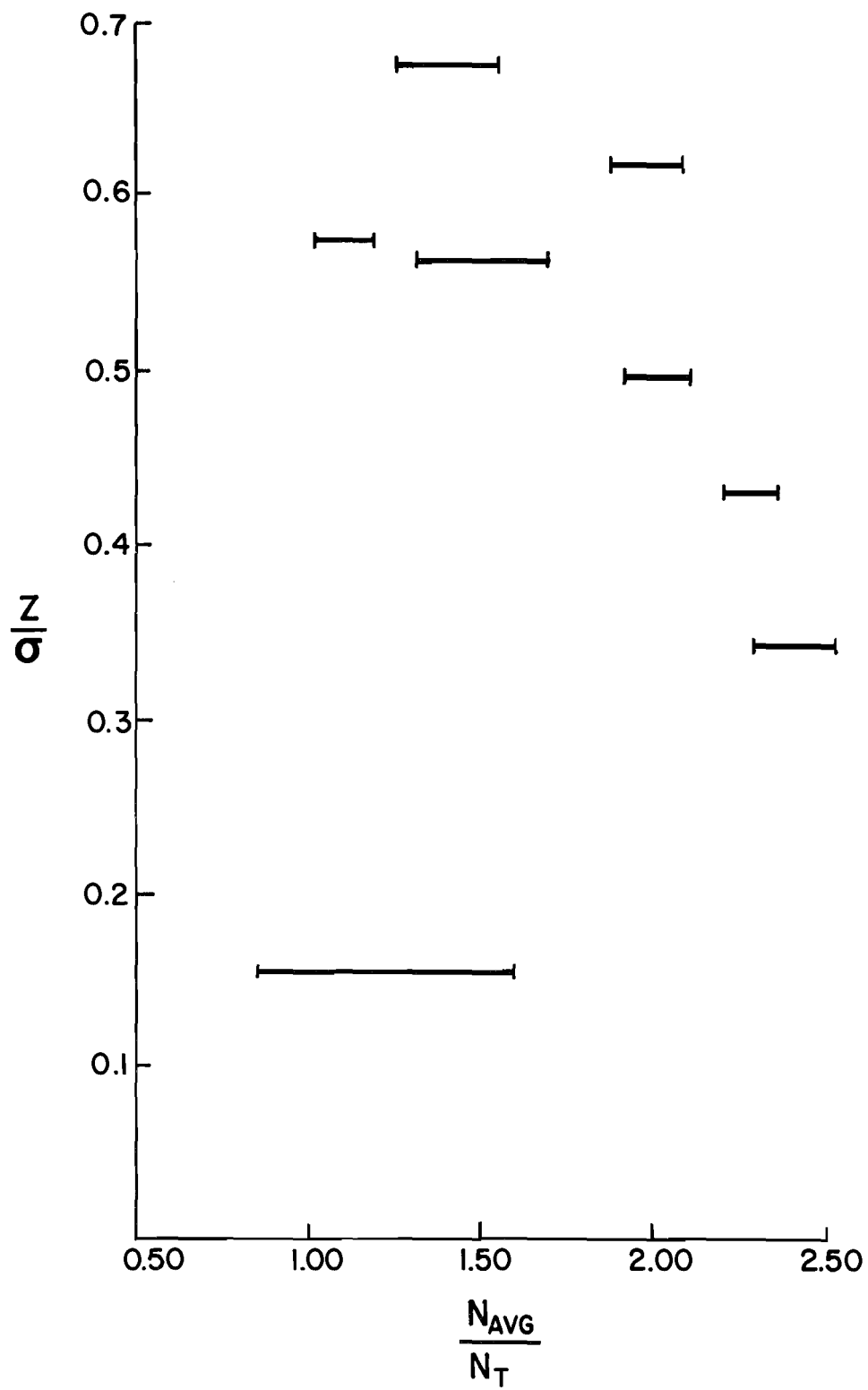Fig. 3.7   Plot of z/σ vs. N_{avg}/N_t

CHAPTER 4: DISCUSSION OF EFFECTIVE STRESS CALCULATION

Three effective stress methods (Miner's, tensile, and Gurney's) were investigated to determine their ability to predict the failure of the SS tests. SS test results indicated that a Miner's effective stress calculation gave unconservative fatigue life prediction. Thus the tensile effective stress method was not considered further as tensile effective stresses for any SS waveform would have an even lower effective stress than the corresponding Miner's effective stress. This lower effective stress would yield a more unconservative fatigue life prediction. On the other hand, Gurney's effective life prediction would appear to give slightly closer fatigue life prediction.

4.1 EVALUATION OF GURNEY'S METHOD

A comparison of the fatigue life prediction based on Gurney's approach and Miner's rule is shown in Table 4.1. The predicted lives from Gurney's approach are in better agreement with the experimental results then the lives predicted from Miner's approach. Miner's approach gave unconservative predictions that were off by a factor of two or more. Gurney's approach gave only four fatigue life predictions that were greater than 10% off on the unconservative side.

The SS test results have been plotted at the cycles to failure using "N", the number of major stress cycles of the major stress range,

TABLE 4.1   COMPARISON OF GURNEY'S PREDICTED FATIGUE LIFE OF
SS TESTING AGANST ACTUAL FATIGUE LIFE

Specimen Number	Nominal			Cycles to Failure $Nx10^3$	Gurney's Predicted Life $x10^3$	Actual Predicted	$\sum \frac{n}{N}$
	r_{major}	p	(v+1)				
SS2207	35	.154	10	183	208	0.880	0.617
SS2208	35	.154	10	339	208	1.630	1.144
SS2209	35	.571	8	141	88	1.602	0.820
SS2210	35	.571	8	164	88	1.864	0.953
SS2411	25	.560	10	394	338	1.166	0.576
SS2412	25	.560	10	504	338	1.491	0.737
SS3204	35	.429	16	85	90	0.944	0.414
SS3205	35	.429	16	91	90	1.011	0.442
SS3306	30	.500	10	187	185	1.011	0.479
SS3307	30	.500	10	195	185	1.054	0.499
SS3408	25	.600	5	393	475	0.827	0.467
SS3409	25	.600	5	436	475	0.918	0.518
SS4305	30	.500	10	181	185	0.978	0.463
SS4311	30	.500	10	199	185	1.076	0.507
SS4306	30	.333	10	225	264	0.852	0.426
SS4309	30	.333	10	204	264	0.773	0.386
SS4307	30	.667	10	133	123	1.081	0.627
SS4308	30	.667	10	164	123	1.333	0.772

σ, in Figs. 4.1, 4.2, and 4.3. Figure 4.1 shows only the SS data with stress sequences "v + 1" equal to 10. Prediction curves based on Gurney's formulation are plotted as dashed lines for each different value of σ shown. In Figs. 4.2 and 4.3, only SS test results with σ equal to 15 ksi and 20 ksi respectively are plotted. Prediction curves of these figures are plotted for each different value of "v + 1". Constant amplitude points are designated by a bar — on the plotted symbol in Figs. 4.1, 4.2, and 4.3. These plots show that the data corresponds well with the prediction curves. Generally, the data falls to the right of its predicted value, meaning that the fatigue life prediction curves are conservative.

Fig. 4.4 shows how well the results of this study and Gurney's experiments [4] correspond to Gurney's fatigue life prediction. The solid line represents full agreement between tests and theory. Both sets of data contain a good deal of scatter. However, most of the scatter is on the conservative side.

4.2 EVALUATION OF A NON-LINEAR DAMAGE MODEL

The test results indicate that the damage caused by the small stress cycles is non-linear. A non-linear damage theory was investigated to explore this effect. Assuming that the damage effect of the major stress cycle, σ, is unaltered and taking "m" to be constant, an effective stress z_{eff} can be calculated which will emulate the non-linear damage by manipulating the S_{re} calculation as follows:
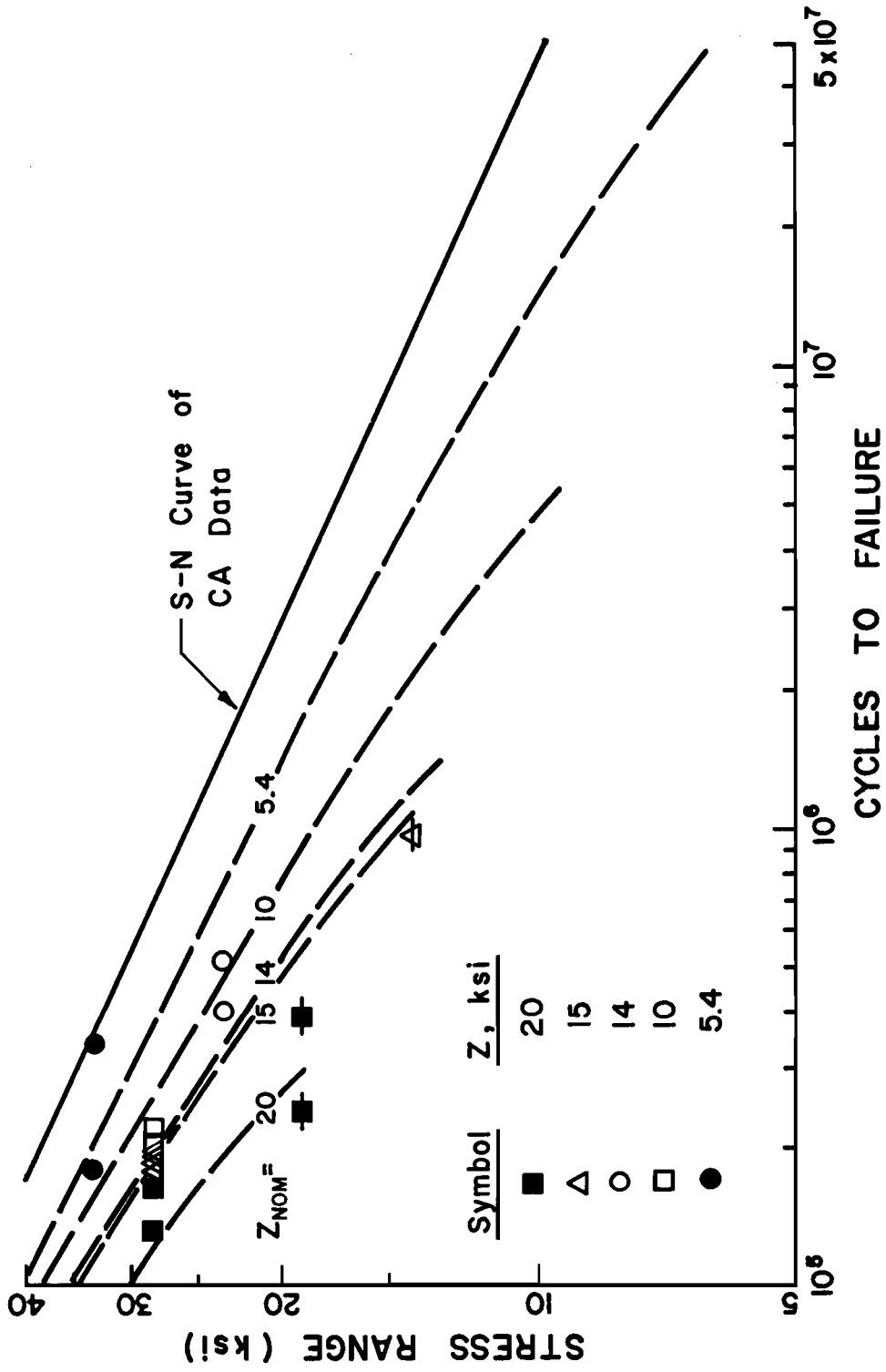
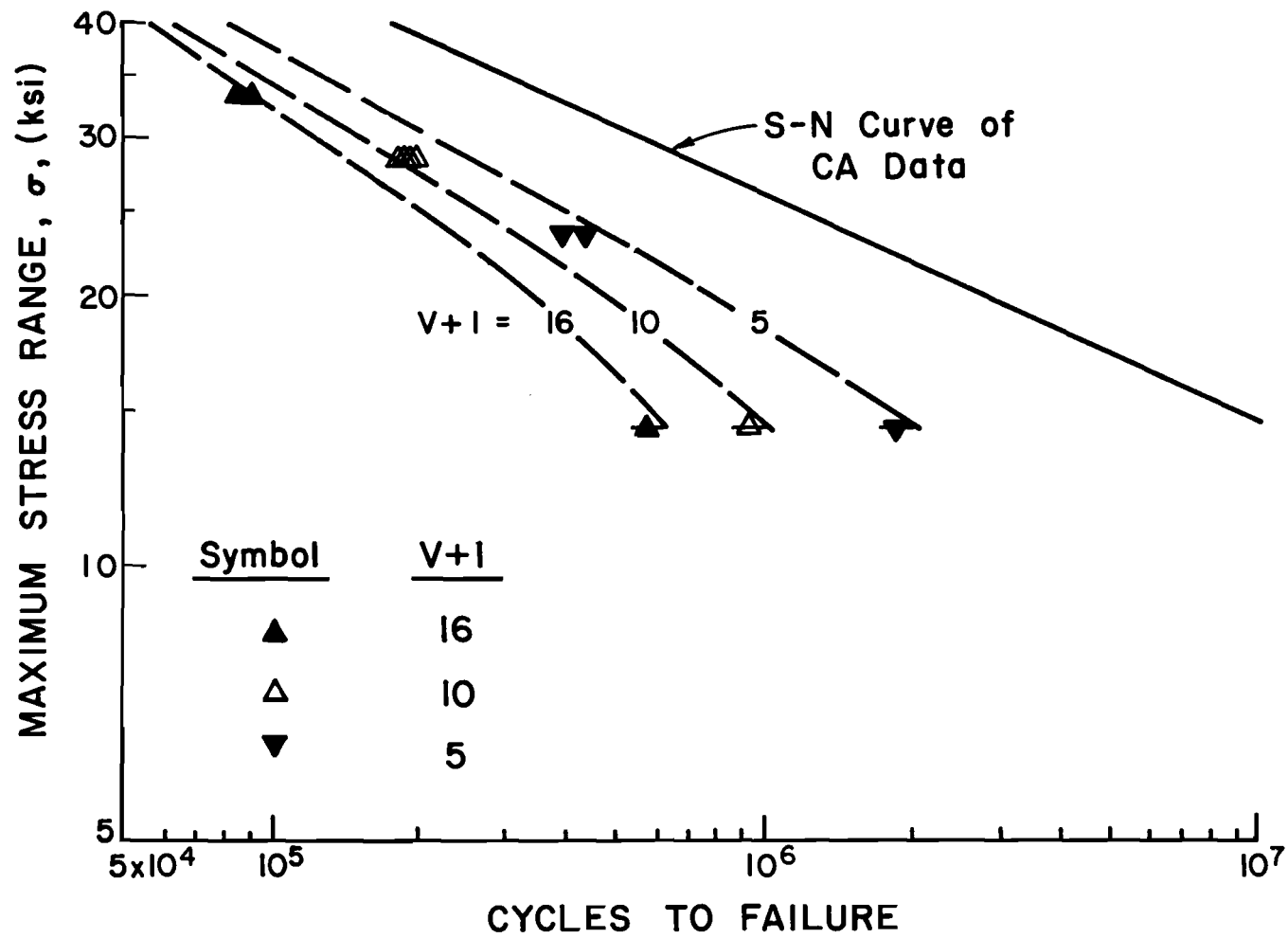Fig. 4.1 SS test results with stress sequences, v + 1, equal to 10

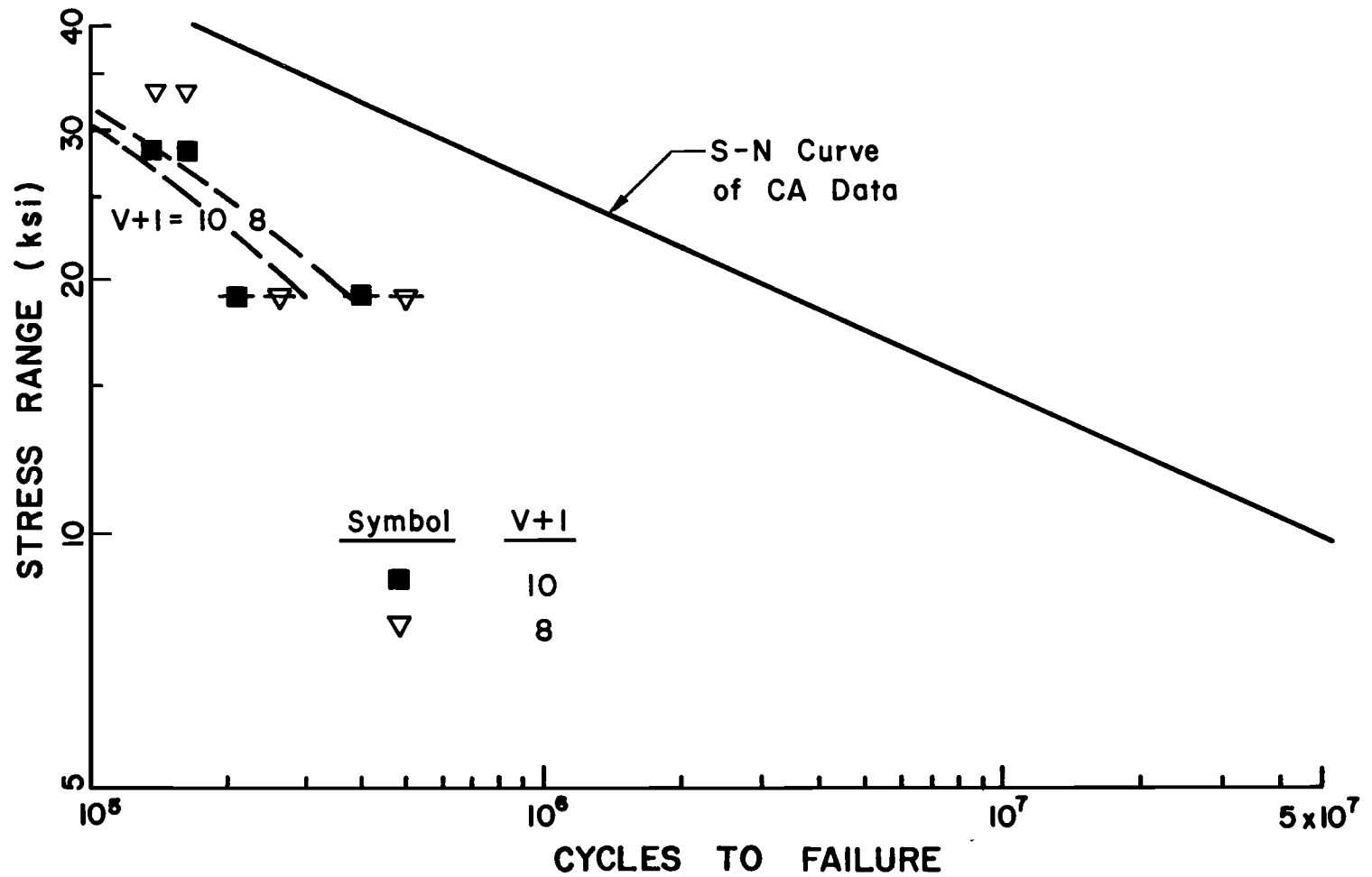Fig. 4.2 SS test results with minor stress range, z, equal to 15 ksi

Fig. 4.3 SS test results with minor stress range, z, equal to 20 ksi

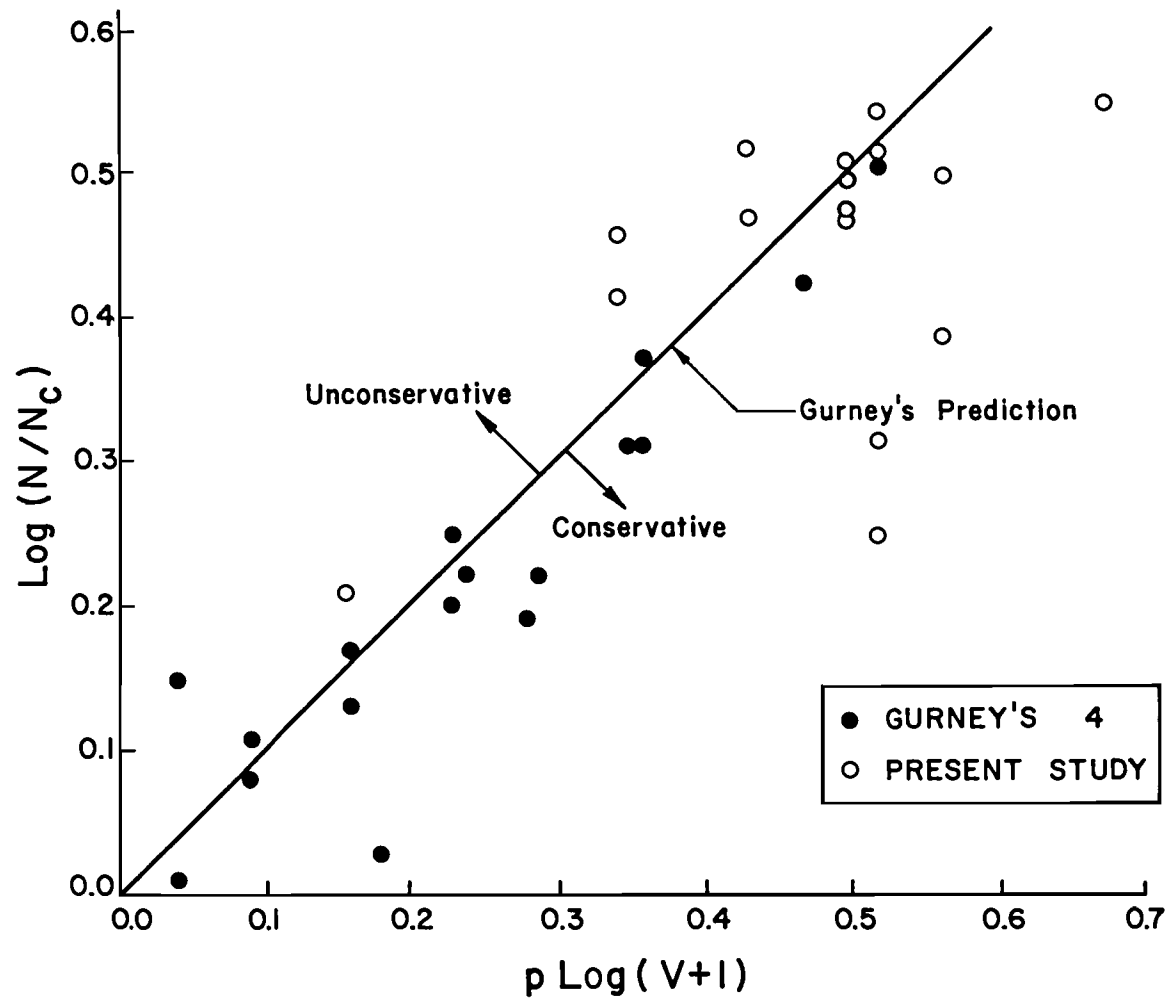Fig. 4.4 Log (N/N_c) vs. p Log (v + 1)

$$S_{re} = \left[\gamma_\sigma \sigma^m + \gamma_z z_{eff}^{\ m} \right]^{1/m} \tag{4.1}$$

and

$$N_t = A \ S_{re}^{-m} \tag{4.2}$$

By substituting the expression of S_{re} in eqn. 4.1 into eqn. 4.2 and solving for z_{eff} gives:

$$z_{eff} = \left[\frac{A}{\gamma_z N_t} - \gamma_\sigma \sigma^m \right]^{1/m} \tag{4.3}$$

Constants "A" and "m" are known from the regression analysis of the CA data. γ_z and γ_σ are fixed for a given test. Therefore, z_{eff} can be calculated.

The ratio z_{eff}/z is plotted in Fig. 4.5 as a function of z/σ for all SS tests. The SS test data for a given test type are plotted as a mean plus or minus the deviation of z_{eff}/z. Rather than disregarding the result of SS2208 because its z_{eff} value was negative, the result was averaged with the z_{eff} from the result of SS2207 and plotted simply as "x". Also included in the plot is Gurney's data which was tested by waveforms with shapes similar to SS waveforms and is plotted as single points. Although Gurney used pulsating tension specimens with a fillet welded attachment, the results of both studies exhibited the same behavior. There is a definite trend in both data sets to have higher relative damage for lower values of z/σ. A simple expression was developed using σ/z to describe this variation in damage. This expression is z_{eff} = SQRT($z\sigma$). A plot of z_{eff}/z = SQRT(σ/z) is shown in Fig. 4.5.

The non-linear damage effect can easily be incorporated into Miner's rule by modifying the effect of the lower stress by the expression SQRT($1/p$), this is the same as SQRT(σ/z), which results in the following effective stress expression for a given SS cycle:
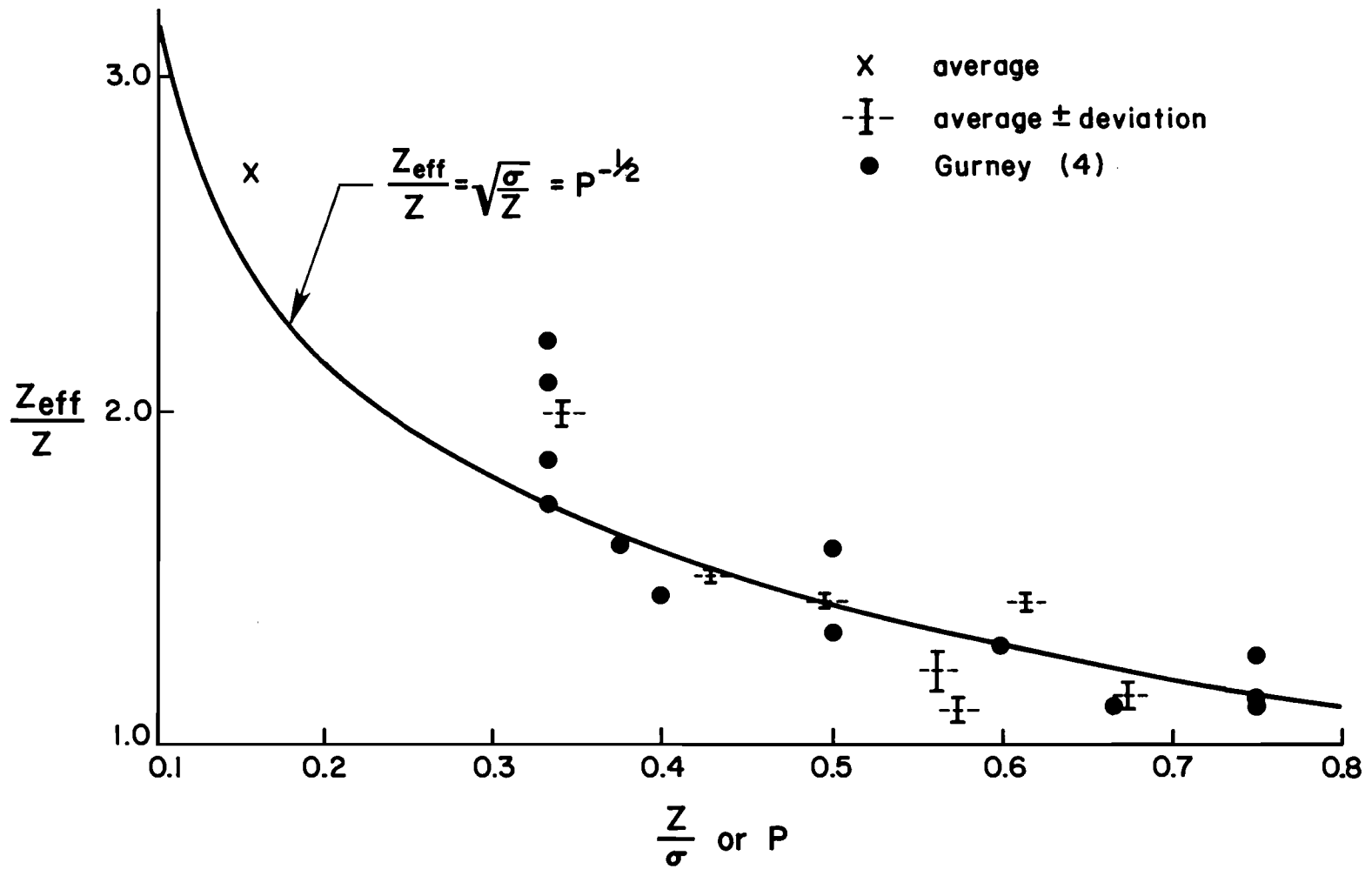
Fig. 4.5 z_{eff}/z vs. z/σ

$$S_i = \left[v(p^{-1/2}z)^m + S_{max}^m \right]^{1/m} \tag{4.4}$$

or

$$S_i = \left[\sum_j \alpha_j (p^{-0.5}S_j)^m \right]^{1/m} \tag{4.5}$$

where α_j is the occurrence of S_j, and p_j is the value S_j/S_{max}. By expressing the effective complex stress, S_i in terms of the occurrence, α, of a stress range rather than in terms of the fractional occurrence, γ, the number of cycles to failure will be expressed as the number of complex cycles, N_c, to failure. At $S_j = S_{max}$, $p_j = 1$ and at $S_j = 0$, $z_{eff} = 0$. Thus eqn. 4.5 meets boundary conditions at $p = 0$ and $p = 1$. By substituting eqn. 4.5 into eqn. 1.11, the following non-linear Miner's expression results.

$$S_{re} = \left[\sum_i \sum_j \gamma_i \alpha_{ij} (p_{ij}^{-0.5} S_{ij})^m \right]^{1/m} \tag{4.6}$$

where γ_i is the fractional occurrence of the complex waveform i. α_{ij} is the occurrence of S_{ij}, and p_{ij} is the value $S_j/S_{max,i}$. $S_{max,i}$ is the S_{max} corresponding to a complex cycle "i". Thus different complex cycles generated from different truck traffic loadings can be accounted.

The non-linear Miner's expression gives fatigue life predictions close to Gurney's expression as shown in Table 4.2 for the different types of SS waveforms tested. Although some of Miner's estimates are closer to the actual prediction than either the Gurney or the non-linear Miner prediction, half of the Miner's estimates are off by a factor of two. Figure 4.6 shows the error associated with the fatigue life prediction based on each of the effective stress methods. Miner's rule had the most unconservative predictions with a mean error of -35%. Both Gurney's and the non-linear Miner's formulas gave comparable results. Their results were mainly on the conservative error side, a
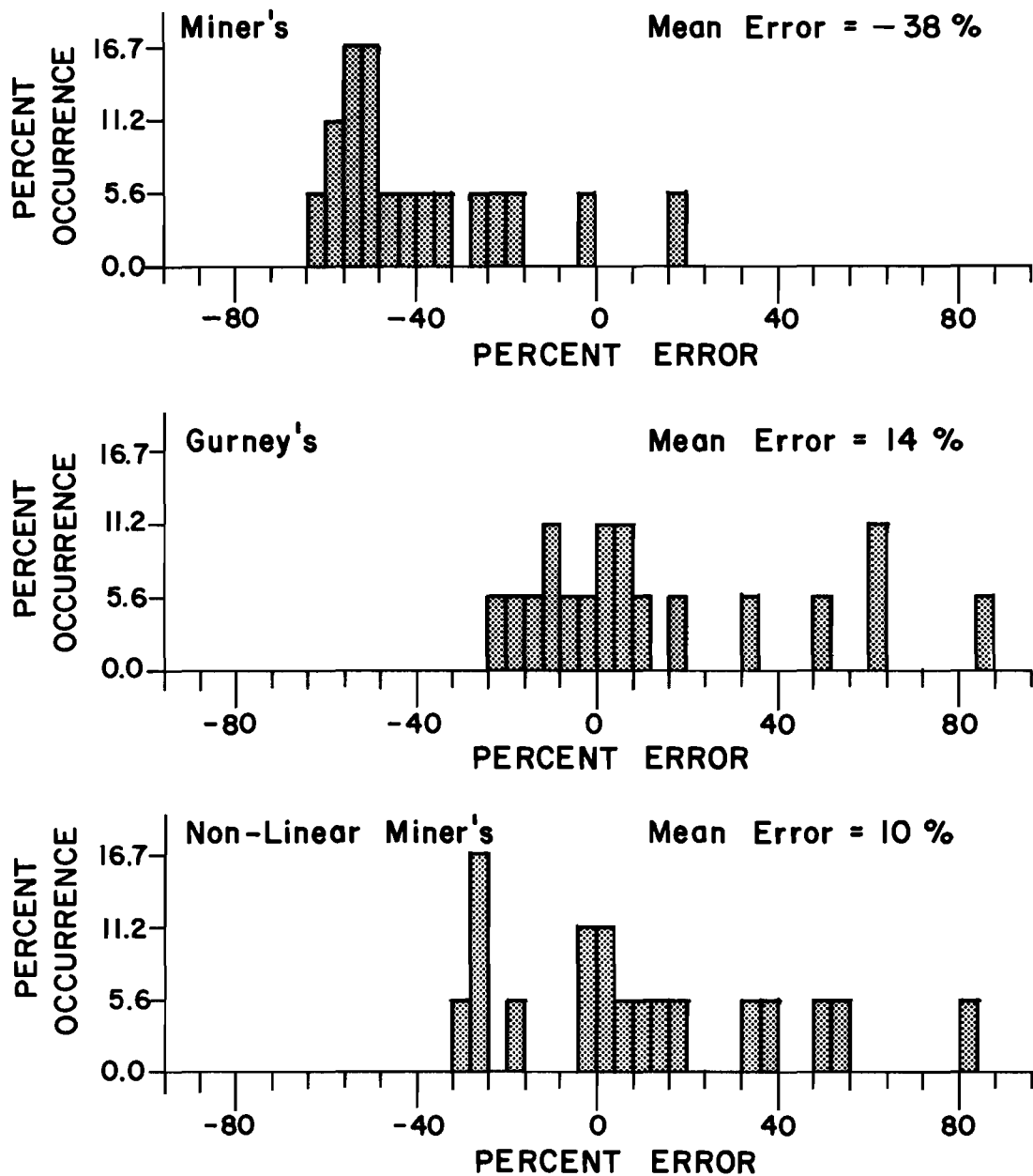
Fig. 4.6 SS testing error histograms of various fatigue life

positive error, with errors ranging from -32% to +86%. The mean error using the non-linear Miner's formula was 10% and using Gurney's formula was 14%. The validity of these two formulations needs to be tested further using waveforms from actual field stress histories.

The type of increase in design stress that a non-linear Miner's approach would cause can be modeled by an SS waveform with $v = 10$ and $p = 0.25$. Setting $m = 3$ and substituting the values of v and p into eqn. 4.4 leads to $S_i = 1.31 \, S_{max}$. This is slightly over 1.30, which is the maximum factor that can be obtained using an AASHTO impact fraction of 0.3. Thus, the use of an AASHTO impact fraction to modify the design stress for bridge fatigue design, may be inadequate.

CHAPTER 5: SUMMARY AND CONCLUSIONS

A research program was carried out to study the influence of high frequency/low stress cycles superimposed on low frequency stress cycles upon the fatigue life of a welded steel tee loaded in bending. The results show that:

1) the damage effect of minor stresses, z, need to be considered in fatigue life prediction.

2) an effective stress, S_{re} based on Miner's rule gives unconservative fatigue life predictions.

3) the damage due to minor stresses, z, are non-linear.

4) Gurney's effective stress, S_{rg} gives relatively conservative fatigue life predictions.

5) an alternate method which provides similar fatigue life predictions as Gurney's for SS waveforms can be obtained by modifying Miner's rule by the expression SQRT(1/p) as follows:

$$S_{re} = \left[\sum_i \sum_j \gamma_i \alpha_{ij} (p_{ij}^{-0.5} S_{ij})^m \right]^{1/m}$$

where p equals the ratio of the minimum stress cycles to the maximum stress in the waveform.

6) the use of the current AASHTO impact fraction, I, can lead to an unconservative bridge fatigue design stress.

Further work should be concentrated on stress waveforms of actual field measured stresses. Assuming that further work continues to find the same fatigue behavior as presented in this study, the non-linear Miner's expression for S_{re} is a practical design formula.

APPENDIX I

The number of cycles that are required of any stress range used in an effective stress approach will not exceed its corresponding constant amplitude fatigue life pending that the power "n" is equal to the constant amplitude slope, "m". This is demonstrated using the expressions for S_{re} and N.

$$S_{re} = \left[\sum_i \frac{n_i}{N} S_i^n \right]^{1/n} \tag{I.1}$$

$$N = A \, S_{re}^{-m} \tag{I.2}$$

Substituting eqn. I.1 into eqn. I.2 gives

$$N = A \left[\sum_i \frac{n_i}{N} S_i^n \right]^{-m/n} \tag{I.3}$$

Setting n = m and solving for A gives

$$A = \sum_i n_i S_i^m \tag{I.4}$$

Expanding eqn. I.4 results in

$$A = n_0 S_0^m + \sum_{i=1}^{j} n_i S_i^m \tag{I.5}$$

Re-arranging terms, n_0 becomes

$$n_0 = \frac{A - \sum n_i S_i^m}{S_0^m} \tag{I.6}$$

or

$$n_0 = A \, S_0^{-m} - \sum n_i \left[\frac{S_i}{S_0} \right]^m \tag{I.7}$$

The corresponding CA value of n_0 is

$$n_0 = A \, S_0^{-m} \qquad (I.8)$$

Since $\qquad A \, S_0^{-m} > A \, S_0^{-m} - \Sigma \, n_i \left[\dfrac{S_i}{S_0}\right]^m \qquad (I.9)$

Then $\qquad n_0(\text{from CA test}) > n_0(\text{from variable amplitude tests}) \qquad (I.10)$

Thus when $m = n$, the number of cycles that are required of any stress range used in an effective stress approach will not exceed its corresponding constant amplitude fatigue life.

REFERENCES

1. Booth, G. S., "Constant Amplitude Fatigue Tests on Welded Steel Joints Performed in Air," Proceedings, European Offshore Steels Research Seminar, Cambridge, U. K., 27-29 November 1978.

2. Committee on Fatigue and Fracture Reliability of the Committee on Structural Safety and Reliability of the Structural Division, "Fatigue Reliability: Variable Amplitude Loading," Journal of the Structural Division, ASCE, Vol. 108, ST1, Proc. Paper 16795, Jan. 1982, pp. 47-69.

3. Gurney, T. R., Fatigue of Welded Structures, Cambridge University Press, Cambridge, U. K., 1979.

4. Gurney, T. R., private communication.

5. Hoadley, Peter W., "Estimation of the Fatigue Life of a Welded Steel Highway bridge from Traffic Data," unpublished MS thesis, The University of Texas at Austin, May 1982.

6. Maeda, Yukio, "Fatigue Cracks of Deep Thin-Walled Plate Girders," Transportation Research Record 664, Bridge Engineering, Vol. 1, 1978, pp. 120-128.

7. Natrella, M. G., Experimental Statistics, Handbook 91, Printing Office, Washington, D.C., 1 August 1963.

8. Ouchida, H., and Nishioka, A., "A Study of Fatigue Strength of Fillet Welded Joints", U.D.C. 620.178.3:621.791.053.26, Hitachi Review, April 1964.

9. Rolfe, S. T., and Barsom, J. M., Fracture and Fatigue Control in Structures--Application of Fracture Mechanics, Prentice-Hall, Inc., Englewood Cliffs, N.J., 1977.

10. Schilling, Klippstein, Barsom, and Blake, "Fatigue of Welded Steel Bridge Members Under Variable-Amplitude Loadings," NCHRP Rep. 188, Transportation Research Board, National Research Council, Washington, D.C., 1978.

11. AASHTO, Standard Specification for Highway Bridges, 11th Edition, Washington, D.C., 1973.

12. Tilly, G. P., and Nunn, D. E., "Variable Amplitude Fatigue in Relation to Highway Bridges," Proc. of the Institution of Mechanical Engineers, Vol. 194, No. 28, 1980.

13. Wildschut, Back, Dortland, and van Leeuween, "Fatigue Behavior of Welded Joints in Air and Sea Water," Proceedings, European Offshore Steels Research Seminar, Cambridge, U. K., 27-29 November 1978.

14. Yamada, K., and Albrect, P., "Fatigue Design of Welded Bridge Details for Service Stresses," Transportation Research Record 607, Transportation Research Board, National Research Council, April 1977.